

Lethal surface ozone concentrations are possible on habitable zone exoplanets

ABSTRACT

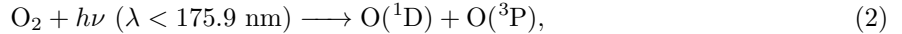
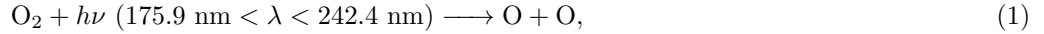
Ozone (O_3) is important for the survival of life on Earth because it shields the surface from ionising ultraviolet (UV) radiation. However, the existence of O_3 in Earth's atmosphere is not always beneficial. Resulting from anthropogenic activity, O_3 exists as a biologically harmful pollutant at the surface when it forms in the presence of sunlight and pollutants. As a strong oxidiser, O_3 can be lethal to several different organisms. Thus, when assessing the potential habitability of an exoplanet, a key part is determining whether toxic gases could be present at its surface. Using the Whole Atmosphere Community Climate Model version 6 (WACCM6; a three-dimensional chemistry-climate model), twelve atmospheric simulations of the terrestrial exoplanet TRAPPIST-1 e are performed with a variety of O_2 concentrations and assuming two different stellar spectra proposed in the literature. Four atmospheric simulations of the exoplanet Proxima Centauri b are also included. Some scenarios for both exoplanets exhibit time-averaged surface O_3 mixing ratios exceeding harmful levels of 40 ppbv, with 2197 ppbv the maximum concentration found in the cases simulated. These concentrations are toxic and can be fatal to life on Earth. In other scenarios, O_3 remains under harmful limits over a significant fraction of the surface, despite there being present regions which may prove inhospitable. In the case that O_3 is detected in a terrestrial exoplanet's atmosphere, determining the surface concentration is an important step when evaluating a planet's habitability.

Keywords: Exoplanets (498) — Exoplanet atmospheres (487) — Habitable planets (695) — Exoplanet atmospheric composition (2021)

1. INTRODUCTION

1.1. Ozone on Earth

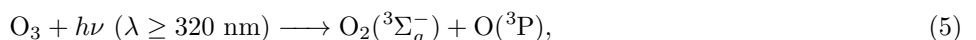
Molecular oxygen (O_2) makes up 21% by volume of Earth's atmospheric composition and is required for aerobic respiration, provides a fuel for combustion, and gives rise to the 'ozone layer'. In an atmosphere with O_2 and sufficient ultraviolet (UV) irradiation at wavelengths shortward of 242.4 nm, O_2 is photodissociated into atomic oxygen (O):



where $h\nu$ represents a photon of frequency ν , and h is Planck's constant. O_2 and O can form ozone (O_3) via the following 3 body reaction:



where M is any third body (usually N_2 or O_2 on Earth due to their relatively high abundance). O_3 can also be destroyed through photolysis, or by reacting with atomic oxygen:



On modern-day Earth, the majority of O₃ resides in the stratosphere, roughly 15 to 35 km above the surface in the ‘ozone layer’ (Brasseur & Solomon 2005). Here, O₃ is beneficial for surface-dwelling life, absorbing biologically harmful UV radiation and providing a partial screen for life exposed to the Sun’s radiation. Even though the majority of Earth’s O₃ is produced in the equatorial stratosphere, there exists a larger column of O₃ at higher latitudes. This is because O₃ is distributed through a seasonal equator-to-pole circulation driven by atmospheric gravity waves, known as the Brewer-Dobson circulation (Butchart 2014). The Brewer-Dobson circulation has been observed to accelerate and decelerate due to climate change (Garcia & Randel 2008; Butchart 2014; Fu et al. 2019), consequently affecting regional composition and temperatures near the tropopause and lower stratosphere.

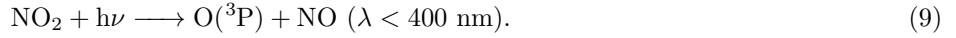
The situation in the troposphere (the lowest atmospheric layer where temperature decreases with altitude) is rather different, because the photolysis rate of O₂ is significantly lower here than in the stratosphere. Near the surface, volatile organic compounds (VOCs) can also contribute to O₃ formation. Hydrocarbon emissions emanate from plants (e.g., isoprene, α-pinene; Chameides et al. 1988; Sharkey et al. 2008) and, on modern day Earth, from anthropogenic activity (e.g., naphthalene, acetone, formaldehyde, and many others; Atkinson 2000). When photooxidation of hydrocarbons occurs in presence of nitrogen oxides, O₃ can eventually be produced through the ‘smog mechanism’ (Haagen-Smit 1952). For example, NO₂ can be produced when OH reacts with a hydrocarbon (Sillman 1999), RH (R is an organic group), producing RO₂ and H₂O:



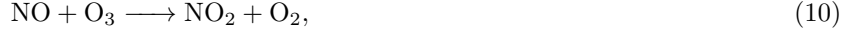
RO₂ leads to NO₂ formation via



Then, NO₂ is photolysed in the presence of UV light:



The O produced can lead to reaction 3, making O₃ at low altitudes. On Earth, surface O₃ is low at night when it is removed through reaction with NO,



and O₃ increases during the day due to photochemistry (Sillman 1999). Reaction 10 is part of a catalytic cycle, where a catalyst (X) leads to the destruction of O₃, but is ultimately not used up in the overall reaction, such that



At the surface, O₃ is considered a pollutant because it causes oxidative stress to plants, insects, and animals, including humans (Avnery et al. 2011; Silva et al. 2013; Valavanidis et al. 2013; Squire et al. 2014; Démares et al. 2022). Oxidative stress is a chemical imbalance between oxidants and reductants inside an organism that can lead to molecular and biological damage (Lykkesfeldt & Svendsen 2007; Sies et al. 2017). It has been demonstrated in many scenarios that O₃ is an antimicrobial agent, capable of microbial inactivation of fungi, viruses, and bacteria (Kim et al. 1999; Guzel-Seydim et al. 2004; Najafi & Khodaparast 2009; Fontes et al. 2012; Epelle et al. 2023; Rojas-Valencia 2011). For instance, the removal of microbiota was demonstrated using ozonation of the air (Epelle et al. 2022), and aqueous O₃ is effective at inactivating microorganisms (Premjit et al. 2022). Additionally, O₃ has been found to be toxic across a wide range of organisms, including guinea pigs, rats, mice, (Stokinger 1965), protozoa, and algae.

It is useful to consider some quantities to illustrate ozone’s danger to life. For example, 40 parts per billion by volume (ppbv) of O₃ is defined by the World Health Organisation (WHO) as a critical limit above which crop yield and species biomass may be reduced (World Health Organization et al. 2000). The WHO stated that significant health effects were exhibited by humans at 80 ppbv (World Health Organization et al. 2000), with O₃ damaging lung function at 100 ppbv for 1 – 8 hours of exposure. Indeed, years of evidence has indicated that long-term exposure to O₃ appears to be related to premature human deaths (Bell et al. 2006; Turner et al. 2016; Sun et al. 2022). For

78 instance, O₃ was attributed to 6,000 premature deaths in the EU in 2013 (Nuvolone et al. 2018), and a modelling study
 79 by Malashock et al. (2022) calculated global O₃-attributable mortality in 2019 was 423,100 deaths (95% confidence
 80 interval of 223,200 – 659,400). The majority (77%) of these were estimated to have occurred in Asia, where ground
 81 level O₃ concentrations were relatively high (Malashock et al. 2022). Furthermore, Feng et al. (2022) estimated that
 82 in East Asia, the reduced crop yield to O₃ pollution costs US\$63 billion annually.

83 1.2. *Ozone on other worlds*

84 If O₃ is detrimental to life on Earth, then the same could be possible for extraterrestrial life. Due to ozone's powerful
 85 oxidising capacity (Menzel 1984; Iriti & Faoro 2007), it is possible that its toxicity to life could be ubiquitous. It is
 86 highly reactive, having a standard electrode potential¹ of 2.075 eV (Kishimoto & Arai 2022), and it ranks amongst
 87 the highest oxidisers (with F₂ the strongest oxidiser at 2.87 eV). O₃, when internal to an organism, causes oxidative
 88 stress by releasing reactive oxygen species, which can then cause damage to proteins, DNA, and ultimately result in
 89 genetic mutations and cell growth that potentially turns into cancer (Klaunig et al. 2010).

90 O₃, its spatial distribution on Earth, and its impact on terrestrial organisms, has been well studied. Less explored
 91 have been the implications of O₃ in exoplanet atmospheres. Hundreds of terrestrial exoplanets, rocky planets orbiting
 92 stars other than the Sun, have been detected in our galaxy. Many of these are in the purported habitable zone (HZ)
 93 around their host star (the region in which liquid water could persist on the surface of a rocky exoplanet; Kasting et al.
 94 1993), although the potential for exoplanets and exomoons to be habitable goes beyond the traditional terrestrial-like
 95 HZ (see e.g., Colose et al. 2019; Tjoa et al. 2020; Madhusudhan et al. 2021). If extraterrestrial life exists, then at
 96 some point in its evolution, it is possible that O₂ could be biologically produced just as it is on Earth, although
 97 there are several scenarios where O₂ could be abiotically produced in high quantities (Wordsworth & Pierrehumbert
 98 2014; Luger & Barnes 2015; Kleinböhl et al. 2018). Either way, O₃ is a molecule of interest because its detection can
 99 indicate the presence of atmospheric O₂. Additionally, O₃ has strong spectroscopic signatures in both direct imaging
 100 and transmission spectra observations at relatively small volume mixing ratios (e.g., between 10⁻⁷ and 10⁻⁵). Due to
 101 this property, some work has shown that in particular scenarios, O₃ may be easier to detect than O₂ (Reinhard
 102 et al. 2017; Kozakis et al. 2022; Cooke et al. 2023). To date, O₃ has not yet been detected in the atmosphere of a
 103 terrestrial exoplanet, so the only estimates of the full O₃ spatial distribution on exoplanets arises from three-dimensional
 104 chemistry-climate simulations.

105 Tidally locked exoplanets are exoplanets that have a rotational period equal to their orbital period (P), such that
 106 they rotate synchronously (Joshi et al. 1997; Showman & Polvani 2011; Pierrehumbert & Hammond 2019). Carone
 107 et al. (2018) simulated tidally locked terrestrial exoplanets with orbital periods of 1 – 100 days, finding that their
 108 atmospheric circulation depends in part on rotation rate. For $P < 25$ days, it was established that stratospheric
 109 transport could occur from the pole to the equator (described as an 'Anti-Brewer Dosbon circulation'), or vice versa,
 110 depending on stratospheric wind breaking and the location of the planetary-scale Rossby waves (e.g., tropical or
 111 extratropical). At rotational periods greater than 25 days, the results from Carone et al. (2018) showed that a
 112 thermally driven circulation between the dayside and nightside could widely distribute air parcels. Yates et al. (2020)
 113 used the Unified Model (UM) to simulate Proxima Centauri b (assuming a terrestrial exoplanet with a 11.18 day
 114 rotation period) in a slab ocean aquaplanet configuration, and found that the nightside O₃ lifetime is much higher than
 115 it is on the dayside. The same conclusion was reached by Proedrou & Hocke (2016), who simulated a tidally locked
 116 Earth with a rotational period of 365 days (no Brewer-Dobson circulation was present on this simulated exoplanet).
 117 Chen et al. (2019) used WACCM4, and reported that the pole-to-equator transport predicted by Carone et al. (2018)
 118 was present in two of their chemistry-climate simulations for terrestrial exoplanets with periods of 4.11 days and 7.91
 119 days, and total irradiation of 1.0 S_0 and 1.1 S_0 , respectively. Recently, Braam et al. (2023) used the UM and found
 120 that O₃ is produced on the dayside and transported to the nightside, with downwelling motions causing O₃ to move
 121 into the troposphere at the positions of the nightside gyres. The use of a slab ocean aquaplanet configuration results
 122 in highly symmetric winds and chemical transport.

123 Only a few studies have commented upon surface O₃ in paleo atmospheres and exoplanet atmospheres. Grenfell et al.
 124 (2013) used a one-dimensional radiative-convective-photochemical model to investigate the atmospheric properties of
 125 super Earths around M0 to M7 stars and with surface gravity of 1 g and 3 g (where $g = 9.81 \text{ m s}^{-2}$). Whilst the
 126 smog mechanism was important for O₃ production around later spectral types, the surface O₃ concentrations did not

¹ the standard electrode potential is "The value of the standard emf of a cell in which molecular hydrogen under standard pressure is oxidized to solvated protons at the left-hand electrode." (McNaught et al. 1997)

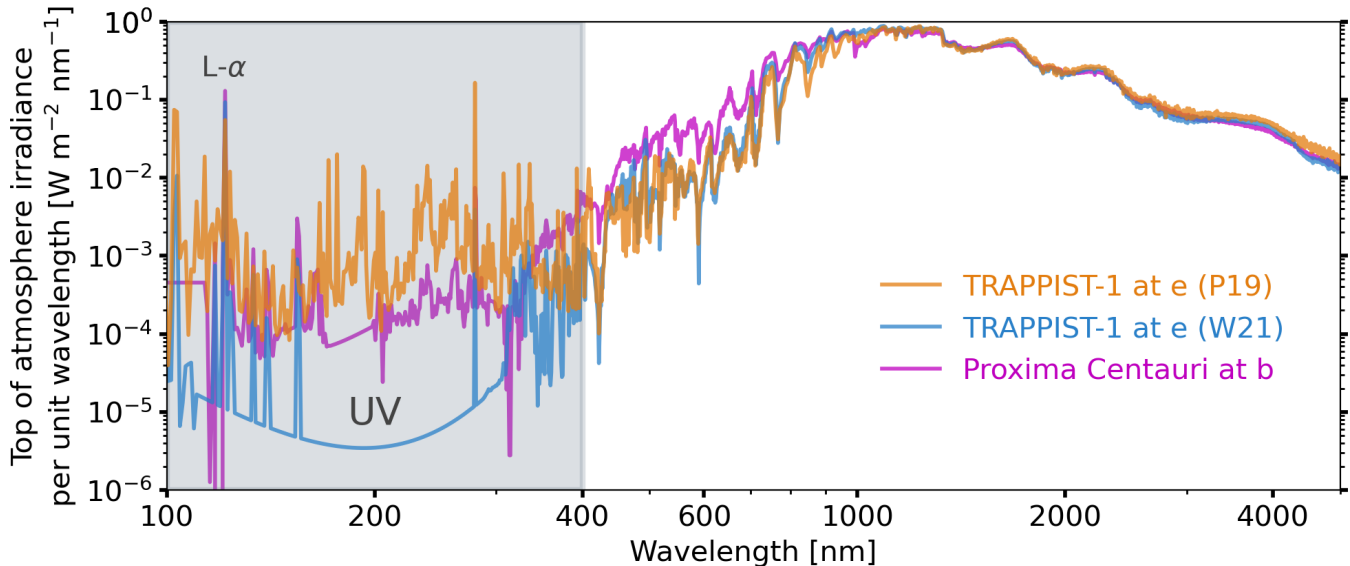


Figure 1. The three stellar input spectra used for the WACCM6 simulations are the PC MUSCLES spectrum (magenta), the Peacock et al. (2019) (P19; orange) and Wilson et al. (2021b) (W21; blue) spectra. The top of atmosphere irradiance per unit wavelength is shown against the wavelength in nm. In the simulations, TRAPPIST-1 e receives 900 W m^{-2} of irradiation ($0.66 S_{\oplus}$, where S_{\oplus} is the total insolation received by the Earth), and Proxima Centauri b receives 884 W m^{-2} ($0.65 S_{\oplus}$). The UV range is highlighted in grey between $100 - 400 \text{ nm}$, and the Lyman- α line is labelled. The average difference between the TRAPPIST-1 spectra in the UV range is a factor of 500, with a difference of up to 5000 in some wavelength bins.

127 exceed harmful levels. Grenfell et al. (2006) used a box model and showed how the smog mechanism could produce
 128 ground-level O_3 up to 3500 ppbv during the Proterozoic (2.4 – 0.541 Gyr ago) on Earth at 1% the present atmospheric
 129 level (PAL) of O_2 . During the Proterozoic, O_2 concentrations could have ranged between $10^{-5} - 1$ times the PAL of
 130 O_2 (Large et al. 2019; Steadman et al. 2020; Lyons et al. 2021).

131 The study by Grenfell et al. (2006) is the only example of a simulated atmosphere which differs to modern Earth
 132 where harmful levels of O_3 have been discussed, although the narrative focused on how O_3 would have shielded the
 133 early Earth from UV radiation. No previous work has discussed the hypothetical dangers from O_3 for extraterrestrial
 134 life on exoplanets and also used a 3D chemistry-climate model which accounts for horizontal transport. This work
 135 presents simulations of the exoplanets TRAPPIST-1 e and Proxima Centauri b using WACCM6, a 3D chemistry-
 136 climate model. Both exoplanets are located in the supposed HZ of their host stars, and TRAPPIST-1 e is a target for
 137 JWST transmission spectra observations. Proxima Centauri b orbits the star Proxima Centauri (M5.5V spectral type,
 138 with a stellar effective temperature of 2,992 K; Pineda et al. 2021), which is the closest star to the Sun (1.3 pc; Gaia
 139 Collaboration et al. 2016), making it an exciting target for future observations (Fowler et al. 2023). TRAPPIST-1
 140 e is a roughly Earth-sized exoplanet orbiting in the HZ around its ultra cool M8V dwarf host star, TRAPPIST-1.
 141 Whilst faint, TRAPPIST-1 is relatively close at a distance of 12.4 pc (40.5 light years). As host of 6 other terrestrial
 142 exoplanets, the TRAPPIST-1 system is a prime target to test theories of planetary system formation and evolution, by
 143 confirming whether atmospheres exist on any of the exoplanets, and characterising their properties if they do. To date,
 144 analysis of observations of the exoplanetary thermal emission with JWST suggests that the two innermost exoplanets,
 145 TRAPPIST-1b and c, have either thin atmospheres, or no atmosphere at all (Zieba et al. 2023; Greene et al. 2023).
 146 Assuming that Earth-like atmospheres exist on both TRAPPIST-1 e and Proxima Centauri b, we investigate the
 147 abundance and distribution of O_3 concentrations in different simulated scenarios, and discuss the implications for the
 148 habitability of oxygenated worlds.

2. SIMULATIONS

149 We use the three-dimensional Earth System Model WACCM6 (Gettelman et al. 2019) to perform twelve simulations
 150 of possible climates of TRAPPIST-1 e, and four possible climate simulations of Proxima Centauri b. WACCM6 is a
 151 configuration of the Coupled Earth System Model (CESM), and we use version 2.1.3 (CESM2.1.3). In each simulation
 152 the initial conditions represent the approximate conditions of Earth's pre-industrial (PI) atmosphere for the year
 153

154 The simulations have the modern ocean and land configuration, a horizontal resolution of 1.875° by 2.5° (96
 155 latitude points and 144 longitude points), and 70 vertical atmospheric levels from 1000 hPa to 4.5×10^{-6} hPa. Both
 156 the atmosphere and ocean models are set up to be fully interactive so that they respond to physical changes such as
 157 temperature. Because it is likely that Proxima Centauri b and TRAPPIST-1 e rotate synchronously (they may be
 158 tidally locked to their host star, although spin-orbit resonance states are plausible; Ribas et al. 2016; Renaud et al.
 159 2021), the substellar point is fixed. This is done by fixing the solar zenith angle in each grid cell. The exoplanet's
 160 obliquity and orbital eccentricity are set to zero. We run WACCM6 with middle atmosphere chemistry which is
 161 described in Emmons et al. (2020), where further details can be found. This chemical mechanism in the WACCM6
 162 simulations has 98 chemical species and 298 chemical reactions, including both the photochemical and heterogeneous
 163 reactions that are necessary to simulate the atmospheric conditions of 1850, and crucially, O₃ chemistry. O₃ pollution
 164 due to VOCs is not simulated. The atmospheric time step, Δt , is 30 minutes. The concentrations of 75 species are
 165 computed using the implicit method, which considers the chemical system at time t and $t + \Delta t$ to evaluate the system
 166 at the future time step $t + \Delta t$ (Sandu et al. 1997). 22 long-lived species are computed with the explicit method,
 167 which calculates the chemical system at a later time $t + \Delta t$ by considering the current system at time t (Brasseur &
 168 Solomon 2005). N₂ is invariant in each simulation, and its mixing ratio in each simulation is adapted to ensure that the
 169 atmosphere maintains a surface pressure of 1,000 hPa. Following the work by Ji et al. (2023), we include absorption
 170 by O₃, O₂, CO₂ and H₂O in the Schumann-Runge bands (175 – 192 nm).

171 ‘Dry deposition’ is the process through which atmospheric trace gases and particulate matter are deposited on
 172 Earth's surface and are removed from the atmosphere, and is an atmospheric sink of O₃. Dry deposition in WACCM6
 173 (Emmons et al. 2020) was updated following Val Martin et al. (2014), and was originally based on a parameterisation

Table 1. The sixteen simulations used in this study are listed. Twelve for TRAPPIST-1 e: six with the P19 spectrum (Peacock et al. 2019) and six with the W21 spectrum (Wilson et al. 2021b). There are four simulations of Proxima Centauri b, where the MUSCLES spectrum of Proxima Centauri (see text for details) is used as stellar input. Each simulation started with the pre-industrial (PI) WACCM6 simulation composition. Each set of six TRAPPIST-1 e simulations includes three with the present atmospheric level of O₂ (0.21 by volume); one where the substellar point is placed over the Pacific Ocean (PI), one where it is placed over Africa (PI SPL), and one where it is not tidally locked and the rotation rate is 1 Earth day (PI noTL). Then, the 10% PAL, 1% PAL, and 0.1% PAL simulations have reduced O₂ mixing ratios from the PI simulation by 10, 100, and 1000 times, respectively. Each of the TRAPPIST-1 e simulations receive a total insolation of 900 W m⁻², and the Proxima Centauri b simulations receive 884 W m⁻² of irradiation. The Proxima Centauri b simulations include the PI, 10% PAL, 1% PAL, and 0.1% PAL cases. The simulated radius and mass of TRAPPIST-1 e are $0.91 R_\oplus$ and $0.772 M_\oplus$, respectively. For Proxima Centauri b, the radius and mass are $1.05 R_\oplus$ and $1.07 M_\oplus$, respectively. The \oplus subscript denotes values relative to the Earth. The orbital parameters assume 0 eccentricity and 0° obliquity, and the table lists the period P and the location of the substellar point (SP) relative to Earth's coordinates (the latitude of the SP is always 0°). Each simulation has been run out for at least 250 model Earth years.

Simulation	Planet	Spectrum	O ₂ mixing ratio [PAL]	Orbital parameters
W21 PI	TRAPPIST-1 e	W21	1.000	$P = 6.1\text{d}$, SP = 180° lon
W21 PI noTL	TRAPPIST-1 e	W21	1.000	$P = 1\text{d}$
W21 PI SPL	TRAPPIST-1 e	W21	1.000	$P = 6.1\text{d}$, SP = 30° lon
W21 10% PAL	TRAPPIST-1 e	W21	0.100	$P = 6.1\text{d}$, SP = 180° lon
W21 1% PAL	TRAPPIST-1 e	W21	0.010	$P = 6.1\text{d}$, SP = 180° lon
W21 0.1% PAL	TRAPPIST-1 e	W21	0.001	$P = 6.1\text{d}$, SP = 180° lon
P19 PI	TRAPPIST-1 e	P19	1.000	$P = 6.1\text{d}$, SP = 180° lon
P19 PI noTL	TRAPPIST-1 e	P19	1.000	$P = 1\text{d}$
P19 PI SPL	TRAPPIST-1 e	P19	1.000	$P = 6.1\text{d}$, SP = 30° lon
P19 10% PAL	TRAPPIST-1 e	P19	0.100	$P = 6.1\text{d}$, SP = 180° lon
P19 1% PAL	TRAPPIST-1 e	P19	0.010	$P = 6.1\text{d}$, SP = 180° lon
P19 0.1% PAL	TRAPPIST-1 e	P19	0.001	$P = 6.1\text{d}$, SP = 180° lon
PCb PI	Proxima Centauri b	PC MUSCLES	1.000	$P = 11.18\text{d}$, SP = 180° lon
PCb 10% PAL	Proxima Centauri b	PC MUSCLES	0.100	$P = 11.18\text{d}$, SP = 180° lon
PCb 1% PAL	Proxima Centauri b	PC MUSCLES	0.010	$P = 11.18\text{d}$, SP = 180° lon
PCb 0.1% PAL	Proxima Centauri b	PC MUSCLES	0.001	$P = 11.18\text{d}$, SP = 180° lon

from Wesely (1989). The parameterisation accounts for variables such as the aerodynamic resistance and the surface resistance, and is influenced by vegetation, if present.

We assume TRAPPIST-1 e receives 900 W m^{-2} of irradiation and that Proxima Centauri b receives 884 W m^{-2} ($0.66 S_0$ and $0.65 S_0$ respectively, where S_0 is the total insolation that the Earth receives). This is consistent with previous work on Proxima Centauri b (Boutle et al. 2017; Yates et al. 2020; Braam et al. 2022; Ridgway et al. 2023) and with the TRAPPIST-1 Habitable Atmosphere Intercomparison project (THAI; Fauchez et al. 2020; Turbet et al. 2022). Proxima Centauri b was detected using the radial velocity method and has a minimum mass measured of $M_P \sin i = 1.07 M_\oplus$ (Faria et al. 2022) only, where M_P is the mass of the exoplanet and i is the inclination angle of the planetary orbit. Therefore, a recently estimated mass-radius relationship from Otegi et al. (2020), given as $R_p = 1.03 M_p^{0.29}$, was used to estimate the planetary radius. Assuming an optimistic mass of $M_P = 1.07 M_\oplus$, this places the radius of Proxima Centauri as $1.05 R_\oplus$, and the surface gravity of Proxima Centauri b at 12.2 m s^{-2} . In our simulations, TRAPPIST-1 e is set to have a mass of $0.772 M_\oplus$ and a radius of $0.91 R_\oplus$, consistent with the THAI project and transit timing variations (TTVs) from Grimm et al. (2018). The surface gravity of TRAPPIST-1 e is therefore set to 9.14 m s^{-2} .

Two semi-empirical stellar spectra were used in the TRAPPIST-1 e simulations. Peacock et al. (2019), henceforth known as P19, modelled the stellar energy distribution (SED) of TRAPPIST-1 and produced model 1A, 2A, and 2B, of which we use model 1A (version 1; Peacock 2020). More recently, Wilson et al. (2021b), hereafter known as W21, used further HST observations to produce a semi-empirical SED of TRAPPIST-1 (version 1; Wilson et al. 2021a) as part of the Mega-MUSCLES series (Froning et al. 2019; Wilson et al. 2021b). Details of their spectra can be found in the aforementioned references. Both the stellar spectra are included here to illustrate how different strengths and shapes of the incoming UV radiation environment can affect the abundance and distribution of surface O_3 . For Proxima Centauri b, we use the GJ 551 MUSCLES (version 2.2; France et al. 2016; Youngblood et al. 2016; Loyd et al. 2016) spectrum as input². GJ 551 is the Gliese–Jahreiß catalog name for Proxima Centauri.

Note that the TRAPPIST-1 e simulations were started in the year 2020, before Agol et al. (2021) published updates to planetary parameters in the TRAPPIST-1 system. For TRAPPIST-1 e, Agol et al. (2021) gave mass and radius values of $0.69 M_\oplus$ and $0.92 R_\oplus$, respectively, meaning the surface gravity would be 8.015 m s^{-2} , instead of 9.14 m s^{-2} as used here. Using these updated values, the scale height of the atmosphere would increase, but we expect that simulations with the parameters from Agol et al. (2021) would produce similar surface O_3 mixing ratios to the ones we present here. Only the minimum mass has been measured for Proxima Centauri b, so it is conceivable that it may have a larger mass and radius than the values used here. Brugger et al. (2016) estimated the radius to be in the range $0.94 - 1.40 R_\oplus$, placing it somewhere between a Mercury-like exoplanet and an ocean-like world. Regardless, with M-dwarf stars being so numerous, it is plausible that somewhere there exists an exoplanet with similar size and instellation, such that these simulations remain useful should Proxima Centauri b eventually be confirmed to have a mass or radius which is significantly larger.

A summary of the simulations is given in Table 1. For TRAPPIST-1 e, six simulations use the P19 (stronger UV) spectrum, and six simulations use the W21 (weaker UV) spectrum. For both exoplanets, atmospheric concentrations of O_2 at the present atmospheric level (PI; 0.21 by volume), 10% PAL, 1% PAL, and 0.1% PAL, are simulated. For TRAPPIST-1 e, we move the substellar point for the 100% PAL simulation between the Pacific Ocean (180° longitude; PI case) and Africa (30° longitude; PI SPL case). We run two simulations which are not tidally locked and have a rotational period of 1 day. Due to computational expense (WACCM6 takes 1,332 core-hours per simulated year to run), we do not simulate the substellar point over land in any of the reduced O_2 cases. Each simulation has been run out for at least 250 model Earth years, and then we present the last year of data (365 Earth days). The full details of the model set-up, alongside simulation scripts, are available via GitHub³.

3. RESULTS

3.1. Surface ozone concentrations

Fig. 2 shows the time-averaged distribution of O_3 at the atmospheric level closest to surface for the cases which have time-averaged surface O_3 mixing ratios of 40 ppbv or greater. We use 40 ppbv as a lower cut-off for harmful

² GJ 551 found at <https://archive.stsci.edu/prepds/muscles/>

³ https://github.com/exo-cesm/CESM2.1.3/tree/main/Tidally_locked_exoplanets

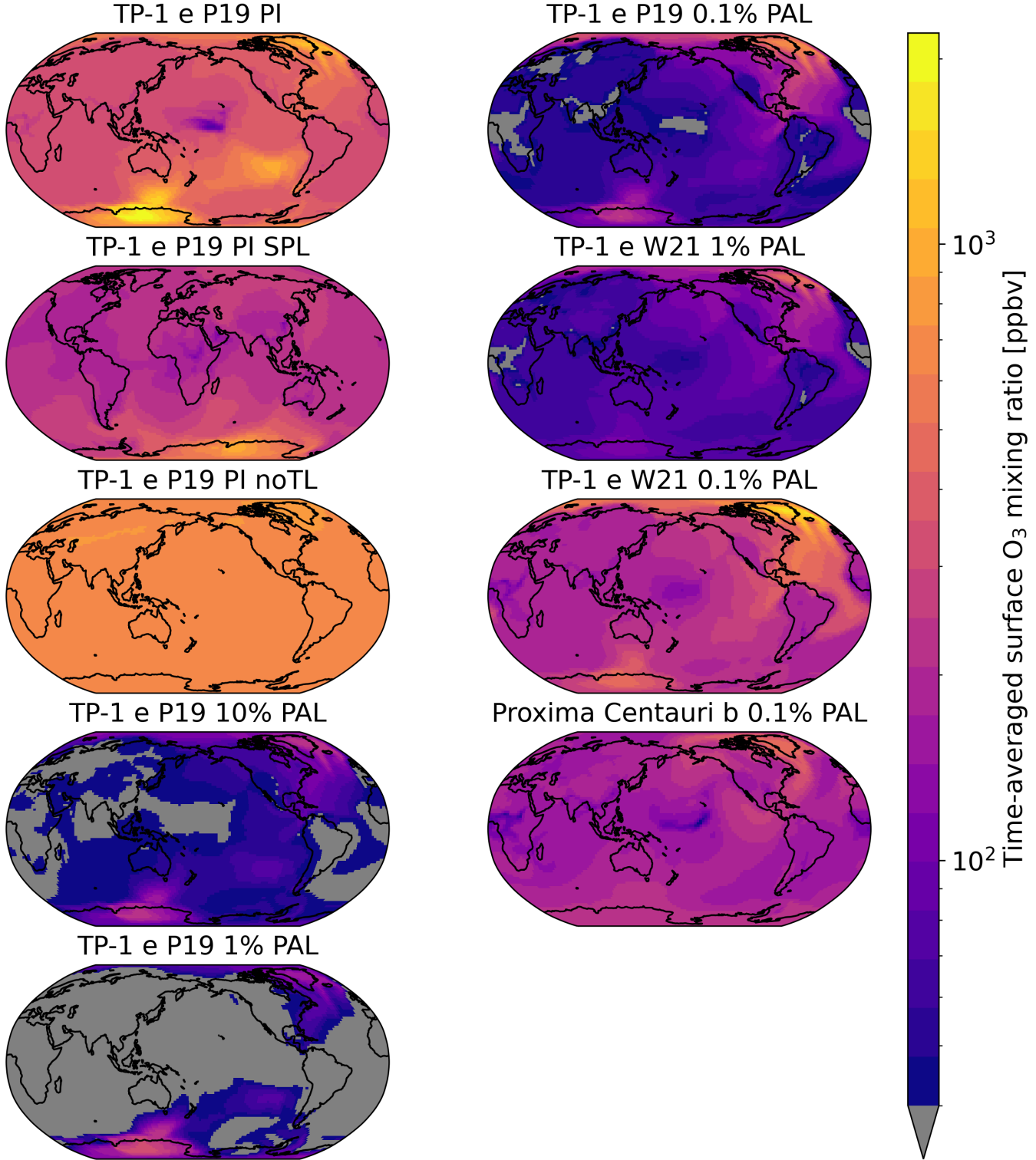


Figure 2. The surface mixing ratio of O_3 , in parts per billion by volume (ppbv), is displayed for the simulations in this work which have time-averaged surface O_3 mixing ratios exceeding 40 ppbv. This includes all TP-1 e P19 cases, the TP-1 e W21 1% PAL and 0.1% PAL simulations, and only a single Proxima Cenaturi b case (0.1% PAL). The PI cases start with an initial pre-industrial atmospheric composition. The PI case has the substellar point placed over the Pacific Ocean, the SPL case has it placed over Africa, and the noTL case is not tidally locked, so that the substellar point moves with time. PAL is the present atmospheric level of O_2 , which is a mixing ratio of 21% by volume. The TP-1 e P19 simulations have stronger incident ultraviolet radiation than the TP-1 e W21 simulations. See Table 1 for a more detailed description of the simulations. Grey indicates where the O_3 mixing ratio is below 40 ppbv and thus at “safe” levels, whilst the different shades of yellow-orange-purple indicate places that exceed 40 ppbv, i.e., these concentrations are known to be harmful to life on Earth. The colour map has a log scale which extends from 40 ppbv to 2200 ppbv.

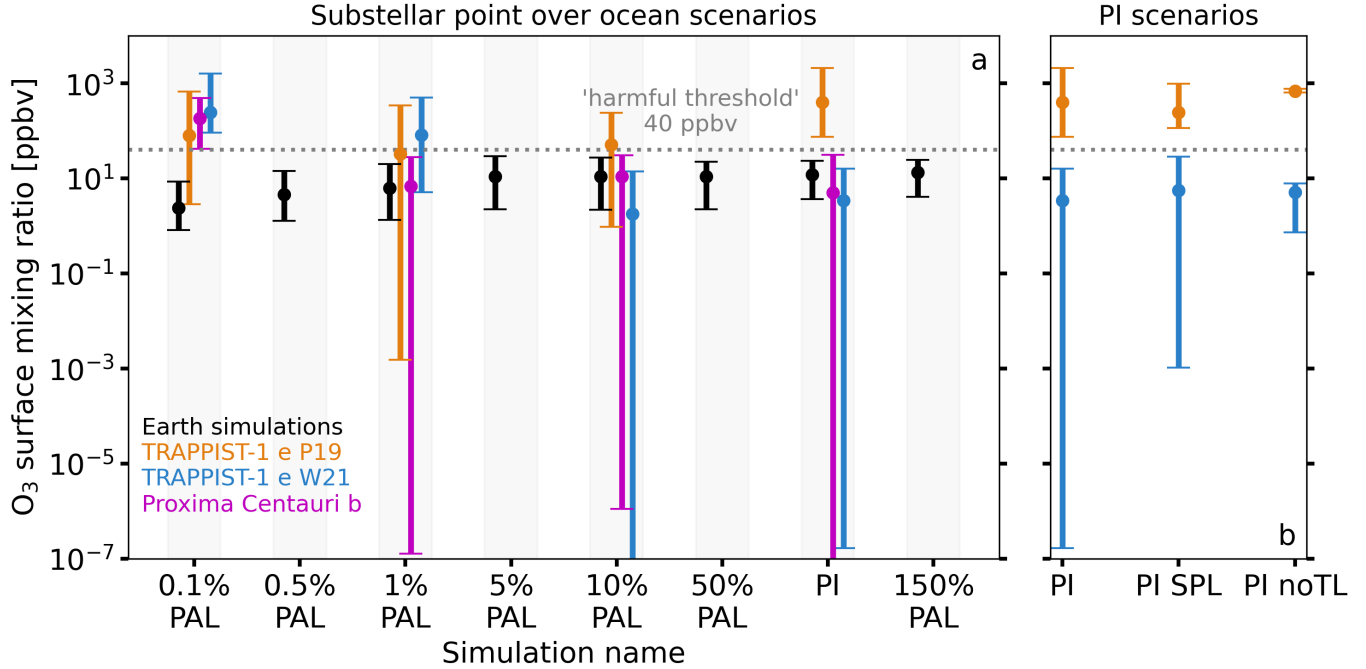


Figure 3. (a) Surface O_3 mixing ratios are presented for the tidally locked P19 (orange) and W21 (blue) TP-1 e simulations, and the PCb simulations (magenta). All of these simulations have the substellar point placed over ocean. The dots show the mean mixing ratio, whilst the top bar shows the maximum, and the bottom bar shows the minimum surface O_3 mixing ratios. Also shown in black are the time-averaged O_3 mixing ratios of data taken from Cooke et al. (2022). The horizontal axis indicates the simulations with a fixed O_2 mixing ratio at the lower boundary, such that the horizontal ticks are categories rather than absolute values (the values are offset from each other for clarity). The grey dotted line indicates the 40 ppbv ‘harmful threshold’, above which O_3 surface mixing ratios are considered dangerous to some forms of life on Earth. (b) The pre-industrial scenarios are compared in the TP-1 e simulations. These include the substellar point over ocean (PI), over land (PI SPL), and the non-tidally locked cases (PI noTL).

levels of surface O_3 (World Health Organization et al. 2000). Grey indicates regions below 40 ppbv, whilst the yellow-orange-purple colour map indicates regions where O_3 exceeds 40 ppbv.

The TRAPPIST-1 e (TP-1 e) P19 PI, PI SPL, no TL, and W21 0.1% PAL simulations everywhere exceed 40 ppbv for surface O_3 . The P19 PI simulation has a maximum mixing ratio of 2197 ppbv, which is the largest surface mixing ratio in all of the simulations presented. In the P19 PI and 0.1% PAL simulations and the W21 0.1% PAL simulation, specific locations (e.g., Antarctica or Greenland) have extremely high mixing ratios, exceeding 1000 ppbv, which is deadly to some organisms on Earth. On the other hand, the W21 PI, PI SPL, and noTL simulations everywhere have O_3 mixing ratios below 40 ppbv, and are not shown. The low O_3 surface concentrations are a consequence of the upper atmosphere efficiently absorbing UV such that insufficient UV reaches altitudes closer to the planetary surface to synthesise enough O_3 . The P19 10%, 1%, and 0.1% PAL simulations, and the W21 1%, simulation, have some areas where O_3 exceeds 40 ppbv, whilst maintaining regions below this limit. For the Proxima Centauri b (PCb) cases, the PI, 10% PAL, and 1% PAL cases have surface O_3 levels below 40 ppbv everywhere. For the 0.1% PAL PCb scenario, surface O_3 everywhere exceeds 40 ppbv and has a global mean mixing ratio of 203 ppbv.

In terms of time variability, the surface O_3 concentrations are not static. Taking the last year of simulated data and averaging each calendar month, the fraction of land for each simulation where surface O_3 concentrations are under 40 ppbv is given in Table 2. For example, the P19 10%, 1%, and 0.1% PAL simulations have monthly O_3 surface concentrations under harmful levels varying between 11.928 – 43.828%, 74.613 – 82.756%, and 4.041 – 9.035% of the total surface area. Considering all these scenarios, the prospect is raised for safe areas on exoplanets which are sheltered from treacherous O_3 concentrations found at other locations. Meanwhile, some locations will fluctuate between toxic and safe levels. Only the P19 PI noTL simulation has surface O_3 mixing ratios that everywhere exceed 40 ppbv throughout the final year of data.

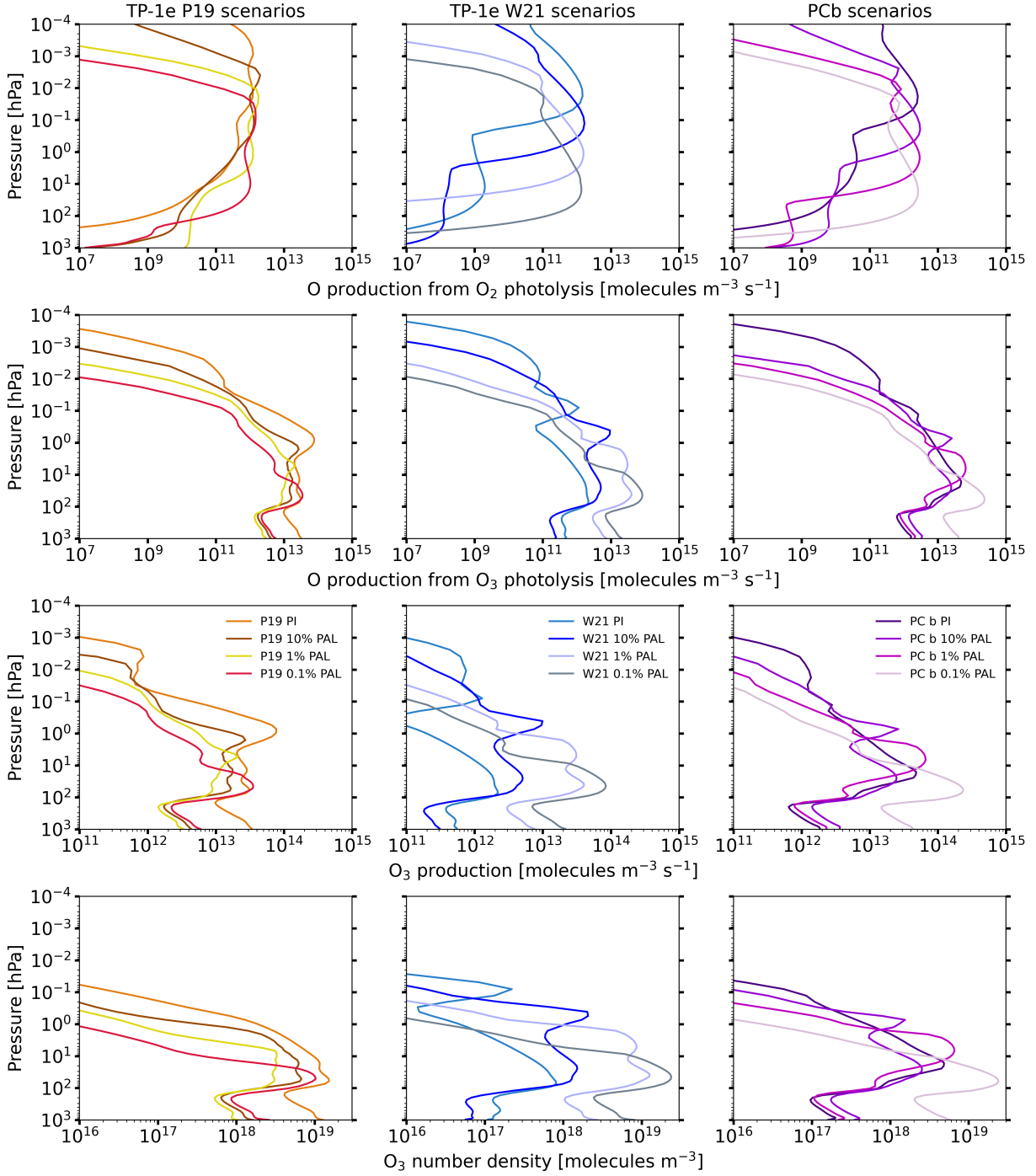


Figure 4. The production of O from O_2 photolysis (top row) and O_3 photolysis (second row) are shown against pressure, with O_3 production (third row) and O_3 number density also shown (bottom row). All profiles are time-averaged global means. The TP-1e PI, 10% PAL, 1% PAL, and 0.1% PAL simulations are shown for both the TP-1 e P19 (orange, brown, yellow, and red, respectively) and TP-1 e W21 (light blue, blue, light blue, and grey, respectively) stellar spectra in the left and middle columns, respectively. The right column show the PCb PI (indigo), 10% PAL (violet), 1% PAL (magenta), and 0.1% PAL (light pink) simulations.

The bars in Fig. 3a indicate the full range of surface O_3 mixing ratios in each of the tidally locked simulations where the substellar point is placed over ocean, with the global mean surface concentrations indicated by the points. Simulations of Earth (using WACCM6) at atmospheric O_2 mixing ratios between 0.1% – 150% PAL from data from

245 Cooke et al. (2022) are given for comparison. Fig. 3b presents the same data for the TP-1 e PI scenarios. The TP-1 e
 246 W21 PI and 10% PAL cases have a large range in surface O₃ concentrations, spanning 7 and 8 orders of magnitude,
 247 respectively. All other TP-1 e simulations span 5 orders of magnitude or less, with the Earth simulations spanning only
 248 one order of magnitude. The PCb simulations span between 9 and 2 orders of magnitude. Whilst both the PI and PI
 249 SPL simulations with the P19 spectrum have harmful O₃ mixing ratios at the surface, the mean surface O₃ mixing ratio
 250 is reduced by 1.7 times when the substellar point is placed over land (PI SPL case). In contrast, the W21 PI SPL case
 251 has 2.0 times the mean surface O₃ mixing ratio of the W21 PI case. Additionally, the noTL cases have a smaller range
 252 than both of the PI tidally locked cases, similar to the Earth simulations. These results imply that surface topography,
 253 the rotation rate, whether or not a diurnal cycle exists, and the position of the substellar point, will be important for
 254 modulating surface concentrations of biologically toxic gases such as O₃. For the PCb scenarios, the PCb 0.1% PAL
 255 case reaches the largest O₃ mixing ratio of 466 ppbv, and everywhere has mixing ratios exceeding 40 ppbv. None of
 256 the Earth simulations have time-averaged O₃ mixing ratios at dangerous levels which is to be expected because the
 257 smog mechanism should not be particularly important on a pre-industrial Earth. The simulations which have surface
 258 O₃ concentrations the most toxic to life are the PI, PI SPL, and PI noTL simulations with the P19 assumed spectrum.
 259 Quantitatively, this corresponds to the simulations where the global mean stratospheric O₃ number density exceeds
 260 7×10^{18} molecules m⁻³. All simulations with O₂ concentrations at 0.1% PAL have toxic mixing ratios exceeding 400
 261 ppbv.

262 3.2. Cause of ozone production at the surface

263 The O₃ profile depends on UV radiation, O₂ number density, O₃ production rates, O₃ loss, and the transport of O₃.
 264 Fig. 4 shows the photolysis rates of O₂ leading to O production (reactions 1 and 2), the photolysis rates of O₃ leading
 265 to O production (reactions 5 and 6), the production rates of O₃ (reaction 3), and the O₃ number density in each
 266 simulation. These quantities are important for understanding where O₃ is produced, and its resulting number density.
 267 O₂ has an approximately constant mixing ratio up until the homopause where gases start to diffusively separate, but
 268 in contrast, the mixing ratio of O increases with altitude until the homopause.

Table 2. The time-averaged and global mean dry deposition flux of O₃ is given in terms of kg m⁻² s⁻¹, for all the exoplanet simulations used in this work, as well as the Earth PI simulation. Dry deposition is a sink for atmospheric surface O₃. The time-averaged and global mean O₃ surface mixing ratios are given. Additionally, the fraction of the surface where O₃ concentrations are under 40 ppbv and thus considered “safe” is given for each simulated exoplanet scenario. The O₃ concentrations vary every calendar month, so the fraction is given as a range over a 1-year period and as a percentage.

Simulation	Time-averaged global mean O ₃ dry deposition flux [kg m ⁻² s ⁻¹]	Time-averaged global mean O ₃ surface mixing ratio [ppbv]	Fraction of surface with O ₃ mixing ratios below 40 ppbv
Earth PI	2.1×10^{-11}	12	N/A
W21 PI	1.0×10^{-12}	3	100.000 – 100.000%
W21 PI noTL	4.3×10^{-15}	5	100.000 – 100.000%
W21 PI SPL	1.3×10^{-14}	6	100.000 – 100.000%
W21 10% PAL	6.2×10^{-13}	2	100.000 – 100.000%
W21 1% PAL	1.8×10^{-11}	82	0.953 – 3.507%
W21 0.1% PAL	4.9×10^{-11}	246	0.000 - 0.331%
P19 PI	9.1×10^{-11}	404	0.000 – 0.080%
P19 PI noTL	4.5×10^{-12}	692	0.000 – 0.000%
P19 PI SPL	4.3×10^{-11}	243	0.000 – 0.029%
P19 10% PAL	1.2×10^{-11}	51	11.928 – 43.828%
P19 1% PAL	6.3×10^{-12}	31	74.613 – 82.756%
P19 0.1% PAL	1.5×10^{-11}	81	4.041 – 9.035%
PCb PI	1.7×10^{-12}	5	99.273 – 100.000%
PCb 10% PAL	4.0×10^{-12}	11	100.000 – 100.000%
PCb 1% PAL	2.2×10^{-12}	7	99.996 – 100.000%
PCb 0.1% PAL	4.6×10^{-11}	203	0.034 – 0.753%

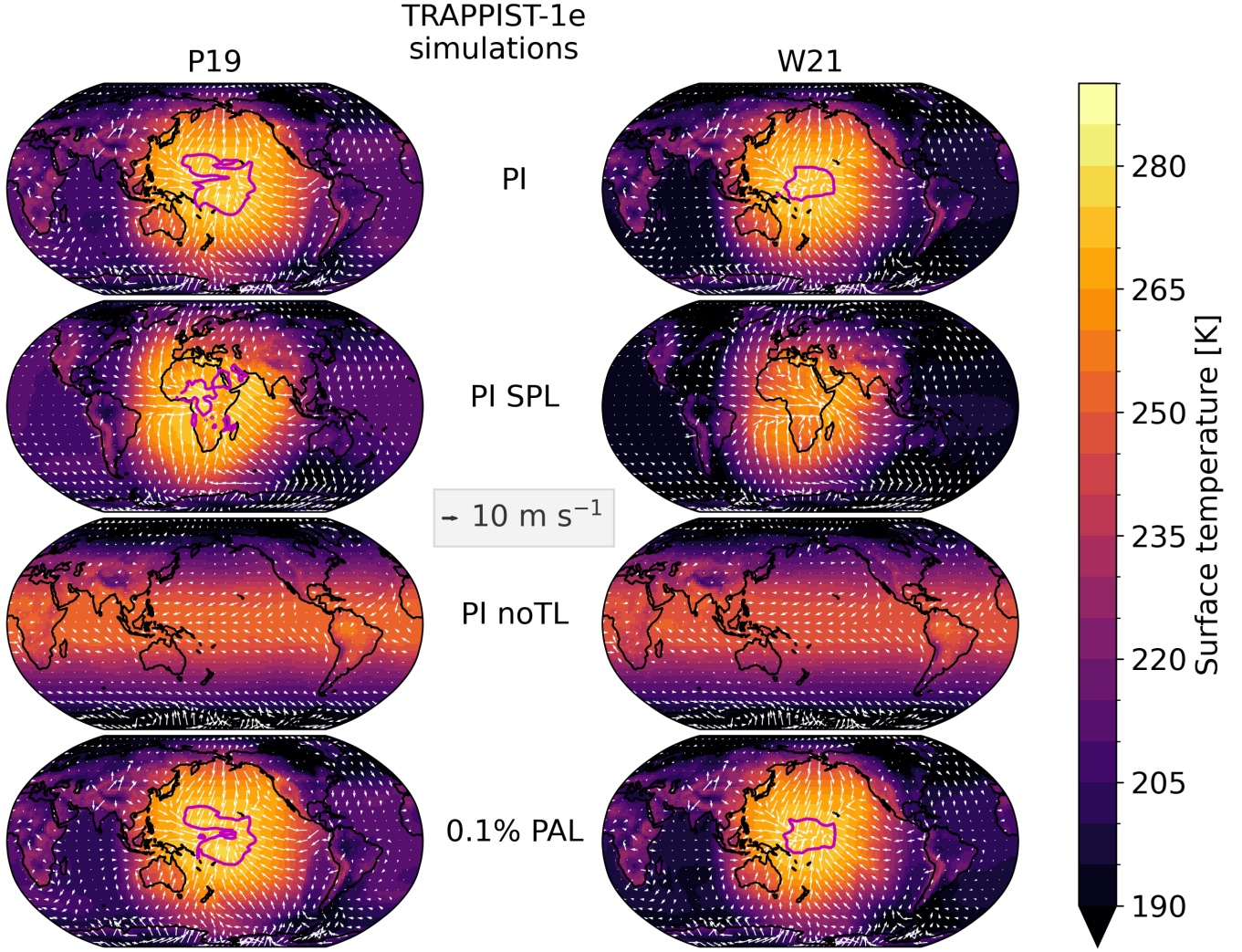


Figure 5. The surface temperature is displayed for the twelve TP-1 e simulations used in this work. The left column shows the P19 simulations and the right column shows the W21 simulations. From top to bottom: PI, PI SPL, PI noTL, and the 0.1% PAL simulations are displayed. White arrows indicate the magnitude and direction of the surface winds. The magenta contours show surface temperatures of 273 K. The 10% PAL and 1% PAL simulations are not shown for brevity, but their surface temperatures are very similar to the PI and 0.1% PAL cases. For scale, a 10 m s^{-1} arrow is shown in the middle of the figure.

In the W21 simulations, as O_2 decreases, the total amount of O_3 in the atmosphere, and at the surface, increases. The opposite is generally true in the P19 simulations, although there is an increase in surface O_3 between 1% PAL and 0.1% PAL. This difference between the P19 and W21 scenarios occurs due to the weak UV radiation in the W21 simulations, and the pressure dependency on the reaction which produces O_3 (reaction 3). When the peak of O_2 photolysis occurs at higher altitudes and thus lower pressure, then O does not react with O_2 as quickly to produce O_3 compared to the rate lower in the atmosphere where the density of the third body, M, is higher. In the P19 cases, whilst the UV can penetrate deeper into the atmosphere when the concentration of O_2 is reduced in the simulations, the availability of O_2 becomes the limiting factor for the production of O_3 , instead of UV radiation. In the PCb cases, there is an intermediate amount of UV radiation compared to the P19 and W21 TP-1 e cases. These PCb cases follow the same trend to the TP-1 e W21 scenarios, with the surface O_3 increasing as O_2 is reduced.

The destruction of O_3 plays an important role in these atmospheres too. Photolysis of O_3 is not counted as a loss of O_3 , because the O produced quickly cycles back to produce O_3 . The peak in O_2 photolysis, O_3 production, and O_3 number density, occurs in each simulation at pressures lesser than 100 hPa (above the troposphere). O_3 formation also

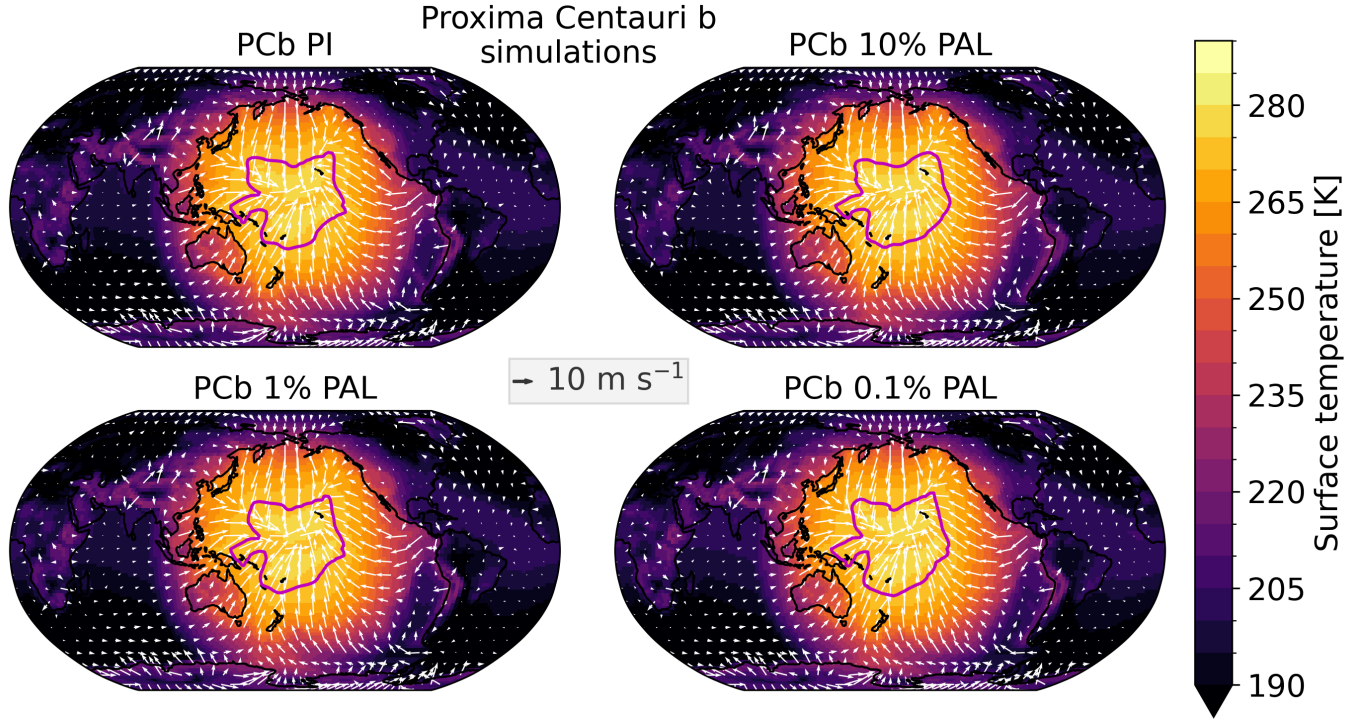


Figure 6. The surface temperature is displayed for the four PCb simulations used in this work: PCb PI (top left), PCb 10% PAL (top right), PCb 1% PAL (bottom left), PCb 0.1% PAL (bottom right). White arrows indicate the magnitude and direction of the surface winds. The magenta contours show surface temperatures of 273 K. For scale, a 10 m s^{-1} arrow is shown in the middle of the figure.

takes place in the troposphere because O₃ photolysis there is fast due to O₃ being present in relatively high quantities. O₃ is being destroyed (by HO_x and NO_x catalytic cycles) and remade in the troposphere, but compared to above the troposphere, its production via O₂, CO₂, NO₂, or H₂O photolysis is significantly slower. It is important to state here that initially in the simulations, O₃ was present in Earth-like quantities throughout the troposphere, and no toxic concentrations existed at the start of the tidally locked simulations.

The atmospheric temperatures and dynamics influence the abundance and distribution of O₃. Fig. 5 shows the surface temperatures (colour map) and surface winds (arrows) in the TP-1 e models, with Fig. 6 showing the same in the PCb models. Several TP-1 e tidally locked simulations have substellar points with temperatures above 273 K, and surface winds converging towards this point (associated with the day-side upwelling at the sub-stellar point), with some of the lowest surface mixing ratios also found near the substellar point. Away from the substellar point, temperatures drop below freezing and can be as low as 170 K on the nightside. The PCb cases have similar surface temperatures and winds because the total irradiance is quantitatively similar to the TP-1 e scenarios ($0.65 S_0$ versus $0.66 S_0$). The cold temperatures result in reduced destruction from catalytic cycles (see reaction 11) which proceed slower at lower temperatures (e.g., from HOx and NOx families), allowing O₃ to persist in relatively high quantities.

Fig. 7 shows the dry deposition flux of O₃ for some of the TRAPPIST-1 e simulations and the Earth PI simulation, and Table 2 shows the global mean dry deposition flux for the Earth PI, TRAPPIST-1 e, and Proxima Centauri b simulations. Dry deposition over snow and ice is slow compared to that over other surfaces (Wesely & Hicks 2000; Helmig et al. 2007; Barten et al. 2023). Additionally, marine surface deposition is slower than land deposition when plant stomata are available to take up O₃ (Ainsworth et al. 2012). The Earth PI simulation has a global mean dry deposition flux of $1.6 \times 10^{-11} \text{ kg m}^{-2} \text{ s}^{-1}$. All TRAPPIST-1 e and Proxima Centauri b simulations have lower loss rates than this, apart from the P19 PI, W21 1% PAL, W21 0.1% PAL and PCb 0.1% PAL simulations. Despite these cases having relatively high rates of dry deposition, all retain harmful concentrations of surface O₃. For the Earth PI case, most O₃ is deposited over land (see Fig. 7). For the exoplanet simulations, the majority of O₃ is deposited near the substellar point, regardless of whether it is placed over land or ocean. The dry deposition flux around the substellar point contributes to the relatively reduced O₃ concentrations at the substellar point (e.g., see the P19 10% and 0.1%

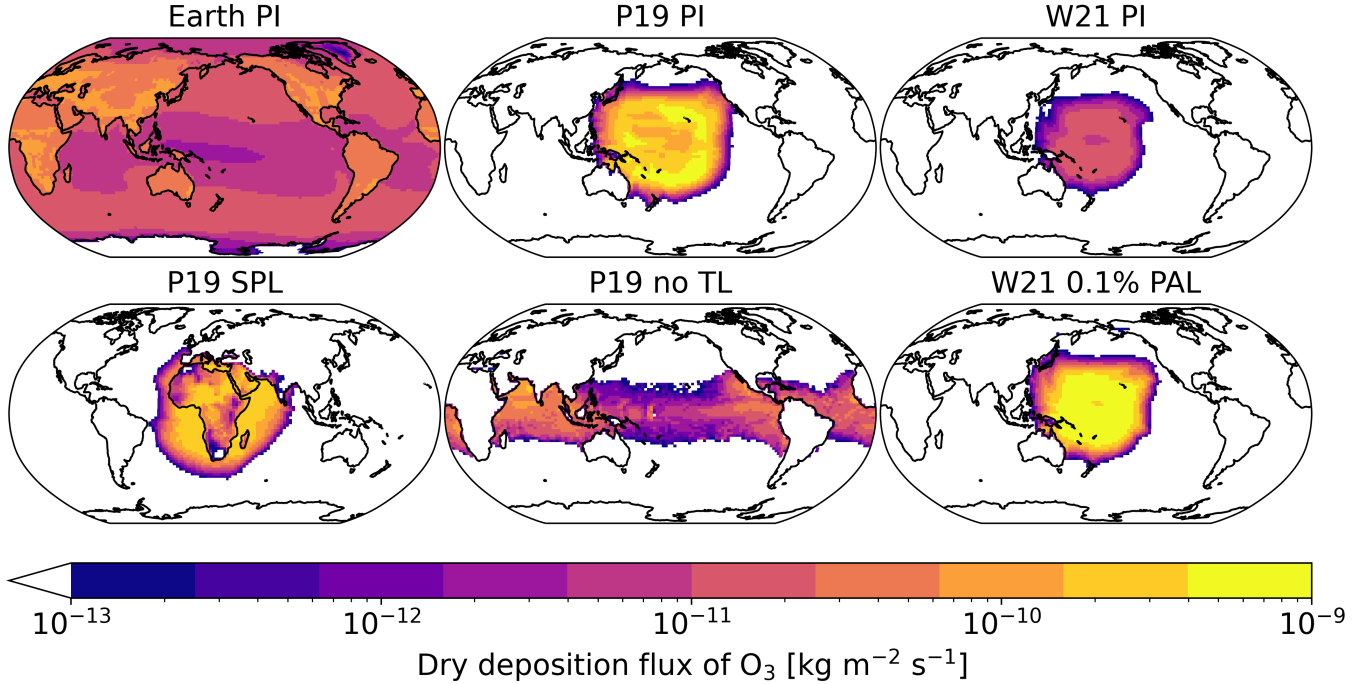


Figure 7. The dry deposition flux of O_3 , given in terms of $\text{kg m}^{-2} \text{s}^{-1}$, is plotted for six simulations: The Earth PI simulation, the TRAPPIST-1 e P19 PI, SPL, noTL, and W21 PI and 0.1% PAL simulations. Yellow indicates relatively large amounts of dry deposition, whilst red indicates relatively low amounts. The white points indicate areas where the dry deposition flux of O_3 is below $10^{-13} \text{ kg m}^{-2} \text{s}^{-1}$.

PAL simulations and W21 1% PAL and 0.1% PAL simulations in Fig. 2). The noTL cases have globally-averaged dry deposition rates that are slower than their PI tidally locked counterparts by a factor of 236 and 20 for the W21 and P19 scenarios, respectively.

To summarise the O_3 distribution in the simulations, O_3 is made primarily in the middle atmosphere on the modelled dayside and the O_3 column maximises at the poles (Cooke et al. 2023). O_3 loss on the nightside and at the poles is slower than the dayside due to relatively low temperatures and a lack of photolysis producing the molecules that become involved in O_3 destroying catalytic cycles. O_3 is lost at the surface due to dry deposition, but the flux is not large enough to mitigate for the dangerous concentrations of O_3 . As an example, in the P19 PI case, the global mean dry deposition flux increases by ≈ 4.3 times greater than the Earth PI case, with a corresponding increase in surface O_3 concentrations of ≈ 33.7 . In the tidally locked cases, the O_3 chemical loss rate at the surface is approximately 2 – 29 times less than the peak stratospheric loss rate. Surface winds (of order 10 m s^{-1}), which are much stronger than vertical winds (of order 0.1 m s^{-1}), transport O_3 across the surface.

We hypothesise that O_3 is transported from where it is produced in the dayside stratosphere to the nightside and towards the poles as discussed in Braam et al. (2023), who simulated Proxima Centauri b assuming an initial condition of a modern-Earth atmosphere. The difference is, in several of our simulations, O_3 accumulates to harmful and lethal quantities. With loss processes in the troposphere less effective than in the stratosphere, the lifetime of surface O_3 increases and enables a build up of toxic O_3 levels. The atmospheric transport throughout the entire atmosphere will be explored in a follow-up paper to confirm whether such a scenario is occurring in the simulations.

4. DISCUSSION

4.1. Prior results for toxic levels of ozone

As far as can be discerned from the presented data (e.g. globally averaged vertical profiles), other 3D simulations of oxygenated exoplanets (Proedrou & Hocke 2016; Way et al. 2017; Chen et al. 2019; Yates et al. 2020), excluding Braam et al. (2022), have not produced surface O_3 mixing ratios above 40 ppbv. This is likely due to the investigated scenarios which differ between each work, although model differences will be important (Ji et al. 2023). Figure 5 in Braam et al. (2022) shows dayside mixing ratios of O_3 reaching ≈ 45 ppbv at the surface. It is worth noting here

that all of these studies, including our simulations, assume a surface pressure of 1 bar (1,000 hPa), so that a mixing ratio of 40 ppbv at 1,000 hPa surface pressure corresponds to a number density of 1.0×10^{18} molecules m⁻³ at 288 K. Chen et al. (2021) used WACCM4 and Ridgway et al. (2023) used the UM (two 3D chemistry-climate models) to investigate the impact of flares and coronal mass ejections on terrestrial exoplanets. The flares significantly perturbed O₃ concentrations⁴, but the changes were in the middle and upper atmosphere and the flares did not cause surface concentrations to exceed 40 ppbv. However, there could be specific cases where flares act to increase O₃ surface concentrations to harmful levels, likely depending on the atmospheric properties, incoming flare strength, and flare frequency.

1D photochemical models have also simulated the impact of flares, CMEs, and cosmic rays on atmospheric chemistry. The calculations in Segura et al. (2010), Grenfell et al. (2012), Tabataba-Vakili et al. (2016), and Tilley et al. (2019), did not demonstrate surface O₃ mixing ratios reaching biologically destructive quantities. The same is true for abiotic O₂ production simulations (Segura et al. 2007; Harman et al. 2015, 2018), although it is unclear in the 100 bar atmosphere from Schwieterman et al. (2016) because surface O₃ mixing ratios are not shown (their figure 1), but O₃ is at 1 ppbv by 10 km and its mixing ratio is strongly decreasing with decreasing height. Other 1D photochemical modelling results have shown that O₃ mixing ratios may exceed harmful levels. For example, Kozakis et al. (2018) used a 1D photochemical model (EXO-Prime; Kaltenegger & Sasselov 2010) to simulate Earth-like exoplanets with various surface pressures of 0.3, 1.0, 1.5, and 2.0 bar, orbiting white dwarf stars (stellar effective temperatures of 4000, 5000, and 6000 K). Almost all simulations had surface O₃ below the 40 ppbv threshold, with only a single simulation (0.3 bar surface pressure and 4000 K stellar effective temperature) exceeding it. However, if it is the concentration (number of molecules per unit volume), rather than the mixing ratio (fractional concentration), which is important, one must take into account the surface density of the atmosphere. Using this criterion, a few more simulations from Kozakis et al. (2018) would be close to 1.0×10^{18} O₃ molecules m⁻³ and therefore potentially dangerous to any surface life present. This was the case for simulated atmospheres around white dwarf stars, however, the 1 bar atmospheres in Kozakis & Kaltenegger (2020) which were simulated around red giant stars did not surpass dangerous surface O₃ concentrations. Regarding smog (see section 1.1 and reactions 7 – 9), Kopparapu et al. (2021) used the 1D photochemical model which is part of ‘Atmos’ (see Arney et al. 2016; Arney 2019) to simulate varying fluxes of NO₂ to test whether it could be used as a signature that extraterrestrial technology existed on an exoplanet. In two simulations (using a Sun-like star and a K6V star with 20× the present Earth flux of NO₂), the surface O₃ mixing ratios were ≈ 90 and ≈ 100 ppbv, respectively. Alongside modern day pollution on Earth due to NOx emissions from vehicles, this study by Kopparapu et al. (2021) demonstrates that the surface fluxes of molecules will be important for determining whether ground level O₃ concentrations reach concerning levels for life. The simulations presented here predict, for the P19 PI case, the highest ozone surface concentrations (7.8×10^{19} molecules m⁻³) compared with other results for exoplanets simulated in the literature.

4.2. Modelling limitations

The model used for the atmospheric simulations is an important factor in these predictions because varying parameterisations and chemical schemes will impact the results. WACCM6 is a model that is tuned to Earth’s atmosphere, land, ice and ocean. WACCM6 accounts for scattering longward of 200 nm, but it doesn’t account for scattering in the Schumann-Runge bands (175 – 192 nm; these wavelengths photolyse O₂ above ∼ 80 km in Earth’s atmosphere), becoming pertinent for Earth-like simulations at O₂ mixing ratios of 1% PAL or less (Ji et al. 2023). In our simulations, WACCM6 accounts for absorption in the Schumann-Runge bands from O₃, O₂, CO₂, and H₂O. The integrated flux in the Schumann-Runge Bands is 1.15, 656, and 26.6 times lower than Earth, for the TP-1 e P19, TP-1 e W21, and PCb cases, respectively. Even with the effect of scattering included, it seems still possible that harmful O₃ surface concentrations could form on the surface of terrestrial exoplanets because all of the P19 simulations have dangerous concentrations of surface O₃. Moreover, the W21 simulations have a relatively low amount of radiation in the Schumann-Runge bands, yet toxic O₃ concentrations are found in the W21 1%, and 0.1% PAL cases.

Ultimately, O₃ mixing ratios are influenced by rates of production, loss, and transport. One sink of surface O₃ is dry deposition, which has been observed to be much slower at night on Earth than during the day (Padro 1996). The lowest dry deposition rates in the tidally locked WACCM6 simulations occur on the nightside, as expected. O₃ dry deposition depends on multiple interlinked parameters which are poorly known (El-Madany et al. 2017), so whether existing dry

⁴ The amount of atmospheric O₃ decreased by a factor of 3 in Chen et al. (2021) for active M dwarf stars, whereas total atmospheric O₃ increased by up to a factor of 20 in Ridgway et al. (2023).

deposition parameterisations can be used for exoplanet simulations is debatable. Thus, how models represent the dry deposition of O₃ will be important for habitability estimates where O₃ concentrations reach potentially toxic levels, with the prescribed topography a significant factor.

4.3. Ozone lethality and surface habitability

The atmospheric and surface temperatures are important variables to consider in terms of planetary habitability. Firstly, in the simulations presented in this work, the vast majority of the surface is frozen or below the freezing temperature of liquid water under 1,000 hPa of surface pressure. Secondly, the temperature has an important influence over O₃ concentrations: colder temperatures quicken the formation of O₃ and concurrently slow the rate of catalytic cycles which destroy O₃. Both parameters will influence the habitability of the exoplanet's surface.

Refuge from the dangerous ozone concentrations may be found in any ocean present. Although it is possible for O₃ to form in water which is irradiated by the Sun (Lushchak 2011), O₃ quickly decomposes in water. Additionally, for disinfection applications, O₃ has to be artificially inserted into water (e.g., via bubble diffusion; Wert et al. 2017) such that it seems unlikely that marine life would be adversely affected by high surface concentrations of O₃ in the air.

Furthermore, different concentrations of O₃ may not cause immediate death for organisms, but rather have much smaller and more limited health effects. This is likely to depend on both the O₃ concentration and the organism in question. We reiterate that O₃ may be ubiquitously toxic, but its known effects on life are limited to observations of terrestrial organisms. Dangerous levels of surface O₃ do not preclude the existence and survival of several different organisms that may have adapted to such an atmosphere, yet it is an important parameter to consider when assessing planetary habitability. For example, some of the scenarios investigated here, such as the TP-1 e P19 PI scenario, which has an average surface mixing ratio of 385 ppbv and a maximum of 2197 ppbv, would be considered uninhabitable for humans.

Indeed, whilst some of these simulated exoplanet climates reside in the HZ because they have surface liquid water, the notion of a Habitable Zone for Complex Life (Schwieterman et al. 2019) is influenced by the presence of toxic gases. So far, the toxic gases that have been suggested are carbon monoxide (CO) and relatively high concentrations of CO₂ (Schwieterman et al. 2019), as well as N₂ at high pressure (e.g., > 2 bar; Ramirez 2020). O₃ can now be added to that list.

4.4. Future work

Future work should aim to determine the parameter space (in UV irradiation, composition, and atmospheric pressure) for which detrimental levels of surface level O₃ may occur. Ideally, 1D photochemical models would be used for this as they are less computationally expensive than 3D models. The use of 1D photochemical models is a viable investigation for non-tidally locked exoplanets. However, for tidally locked exoplanets, where O₃ is transported to the nightside and shielded from destruction (Proedrou & Hocke 2016; Yates et al. 2020; Braam et al. 2023), 3D chemistry-climate models will be needed to predict where surface O₃ concentrations maximise due to atmospheric dynamics. Additionally, one could explore various topographies, gravitational accelerations, and several different atmospheric compositions (e.g., H₂O or CO₂ dominated). As the exoplanets simulated here have limited areas where surface temperatures are above 273 K (and some have no surface temperatures above 273 K), subsequent research could investigate the parameter space with warmer exoplanets to determine how surface O₃ concentrations are affected. Examples of other 3D models that could investigate this chemical phenomenon are LMD-g (Yassin Jaziri et al. 2022), ROCKE-3D (Way et al. 2017), and the Unified Model (Boutle et al. 2017). Once a chemical scheme is implemented, the LFRic-Atmosphere model could also be used (Sergeev et al. 2023). Atmospheres with high O₂, CO₂, or H₂O mixing ratios and sufficient UV may develop an O₃ layer close to the surface because photodissociation could produce O₂ and O molecules which lead to O₃ formation. This may result in potentially dangerous levels of O₃ for any extraterrestrial life present on the surface in such conditions.

5. CONCLUSIONS

This work used WACCM6 to simulate the climate of two exoplanets: TRAPPIST-1 e and Proxima Centauri b. For each exoplanet, we considered O₂ mixing ratios between 0.1% PAL and 100% PAL. Additionally, two different stellar spectra were used for the TRAPPIST-1 e cases to investigate the effect on surface O₃ due to their large differences in the strength of incoming UV radiation. In multiple simulations, O₃ exceeds surface concentrations of 40 ppbv, with maximum time-averaged concentrations reaching up to 2197 ppbv in the TP-1 e P19 PI case. Such concentrations are

harmful to life on Earth and may be potentially fatal through oxidative stress. In these simulated atmospheres, O₃ exists not as a pollutant, but as a consequence of the planetary atmospheric conditions, such as the 1,000 hPa surface pressure, the incoming UV strength and shape, and the O₂ number density vertical profile. Our work suggests the potential presence of toxic O₃ concentrations should be included when evaluating the habitability of an exoplanet.

The simulations examined in this exploratory work represent a small proportion of the parameter space in which atmospheres may form relatively high O₃ concentrations at the surface. Different planetary rotation rates, topography, atmospheric pressures, total irradiation and UV irradiation environments, as well as various chemical fluxes from the surface to the atmosphere, should all be explored. Upcoming work should consider the potential presence of high surface concentrations of O₃ when simulating oxygenated atmospheres. If O₃ is detected in any future observations of terrestrial exoplanet atmospheres, ascertaining the O₃ surface concentration should be incorporated into frameworks that aim to determine planetary habitability and decide on the most promising targets for follow-up observations (see e.g., Truitt et al. 2020; Méndez et al. 2021; Safonova et al. 2021). In practise, this will require a combination of planetary modelling, transmission and direct imaging spectra, as well as precise knowledge of the UV irradiation environment of the atmosphere. 3D chemistry-climate models are essential for understanding how transport can create areas with comparatively lower and thus safer O₃ concentrations. Just as on Earth, the entire surface does not need to be hospitable for life to flourish.

REFERENCES

- Agol, E., Dorn, C., Grimm, S. L., et al. 2021, PSJ, 2, 1, doi: [10.3847/PSJ/abd022](https://doi.org/10.3847/PSJ/abd022)
- Ainsworth, E. A., Yendrek, C. R., Sitch, S., Collins, W. J., & Emberson, L. D. 2012, Annual review of plant biology, 63, 637
- Arney, G., Domagal-Goldman, S. D., Meadows, V. S., et al. 2016, Astrobiology, 16, 873, doi: [10.1089/ast.2015.1422](https://doi.org/10.1089/ast.2015.1422)
- Arney, G. N. 2019, ApJL, 873, L7, doi: [10.3847/2041-8213/ab0651](https://doi.org/10.3847/2041-8213/ab0651)
- Atkinson, R. 2000, Atmospheric Environment, 34, 2063, doi: [10.1016/S1352-2310\(99\)00460-4](https://doi.org/10.1016/S1352-2310(99)00460-4)
- Avnery, S., Mauzerall, D. L., Liu, J., & Horowitz, L. W. 2011, Atmospheric Environment, 45, 2284, doi: [10.1016/j.atmosenv.2010.11.045](https://doi.org/10.1016/j.atmosenv.2010.11.045)
- Barten, J. G., Ganzeveld, L. N., Steeneveld, G.-J., et al. 2023, Elem Sci Anth, 11, 00086
- Bell, M. L., Peng, R. D., & Dominici, F. 2006, Environmental health perspectives, 114, 532
- Boutle, I. A., Mayne, N. J., Drummond, B., et al. 2017, A&A, 601, A120, doi: [10.1051/0004-6361/201630020](https://doi.org/10.1051/0004-6361/201630020)
- Braam, M., Palmer, P. I., Decin, L., Cohen, M., & Mayne, N. J. 2023, MNRAS, 526, 263, doi: [10.1093/mnras/stad2704](https://doi.org/10.1093/mnras/stad2704)
- Braam, M., Palmer, P. I., Decin, L., et al. 2022, MNRAS, 517, 2383, doi: [10.1093/mnras/stac2722](https://doi.org/10.1093/mnras/stac2722)
- Brasseur, G. P., & Solomon, S. 2005, Aeronomy of the Middle Atmosphere: Chemistry and Physics of the Stratosphere and Mesosphere
- Brugger, B., Mousis, O., Deleuil, M., & Lunine, J. I. 2016, ApJL, 831, L16, doi: [10.3847/2041-8205/831/2/L16](https://doi.org/10.3847/2041-8205/831/2/L16)
- Butchart, N. 2014, Reviews of geophysics, 52, 157
- Carone, L., Keppens, R., Decin, L., & Henning, T. 2018, MNRAS, 473, 4672, doi: [10.1093/mnras/stx2732](https://doi.org/10.1093/mnras/stx2732)
- Chameides, W. L., Lindsay, R. W., Richardson, J., & Kiang, C. S. 1988, Science, 241, 1473, doi: [10.1126/science.3420404](https://doi.org/10.1126/science.3420404)
- Chen, H., Wolf, E. T., Zhan, Z., & Horton, D. E. 2019, ApJ, 886, 16, doi: [10.3847/1538-4357/ab4f7e](https://doi.org/10.3847/1538-4357/ab4f7e)
- Chen, H., Zhan, Z., Youngblood, A., et al. 2021, Nature Astronomy, 5, 298, doi: [10.1038/s41550-020-01264-1](https://doi.org/10.1038/s41550-020-01264-1)
- Colose, C. M., Del Genio, A. D., & Way, M. J. 2019, ApJ, 884, 138, doi: [10.3847/1538-4357/ab4131](https://doi.org/10.3847/1538-4357/ab4131)
- Cooke, G., Marsh, D., Walsh, C., & Youngblood, A. 2023, arXiv preprint arXiv:2309.15239
- Cooke, G. J., Marsh, D. R., Walsh, C., Black, B., & Lamarque, J. F. 2022, Royal Society Open Science, 9, 211165, doi: [10.1098/rsos.211165](https://doi.org/10.1098/rsos.211165)
- Cooke, G. J., Marsh, D. R., Walsh, C., Rugheimer, S., & Villanueva, G. L. 2023, MNRAS, 518, 206, doi: [10.1093/mnras/stac2604](https://doi.org/10.1093/mnras/stac2604)
- Démaraux, F., Gibert, L., Creusot, P., Lapeyre, B., & Proffit, M. 2022, Science of the Total Environment, 827, 154342, doi: [10.1016/j.scitotenv.2022.154342](https://doi.org/10.1016/j.scitotenv.2022.154342)
- El-Madany, T., Niklasch, K., & Kleemann, O. 2017, Atmosphere, 8, 175, doi: [10.3390/atmos8090175](https://doi.org/10.3390/atmos8090175)
- Emmons, L. K., Schwantes, R. H., Orlando, J. J., et al. 2020, Journal of Advances in Modeling Earth Systems, 12, e2019MS001882, doi: [10.1029/2019MS001882](https://doi.org/10.1029/2019MS001882)
- Epelle, E. I., Macfarlane, A., Cusack, M., et al. 2023, Chemical Engineering Journal, 454, 140188

- 506 —. 2022, Journal of Microbiological Methods, 194, 106431
 507 Faria, J. P., Suárez Mascareño, A., Figueira, P., et al. 2022,
 508 A&A, 658, A115, doi: [10.1051/0004-6361/202142337](https://doi.org/10.1051/0004-6361/202142337)
 509 Fauchez, T. J., Turbet, M., Wolf, E. T., et al. 2020,
 510 Geoscientific Model Development, 13, 707,
 511 doi: [10.5194/gmd-13-707-2020](https://doi.org/10.5194/gmd-13-707-2020)
 512 Feng, Z., Xu, Y., Kobayashi, K., et al. 2022, Nature Food,
 513 3, 47
 514 Fontes, B., Cattani Heimbecker, A. M., de Souza Brito, G.,
 515 et al. 2012, BMC infectious diseases, 12, 1
 516 Fowler, J., Haffert, S. Y., van Kooten, M. A. M., et al.
 517 2023, arXiv e-prints, arXiv:2309.00725,
 518 doi: [10.48550/arXiv.2309.00725](https://doi.org/10.48550/arXiv.2309.00725)
 519 France, K., Loyd, R. O. P., Youngblood, A., et al. 2016,
 520 ApJ, 820, 89, doi: [10.3847/0004-637X/820/2/89](https://doi.org/10.3847/0004-637X/820/2/89)
 521 Froning, C. S., Kowalski, A., France, K., et al. 2019, ApJL,
 522 871, L26, doi: [10.3847/2041-8213/aaffcd](https://doi.org/10.3847/2041-8213/aaffcd)
 523 Fu, Q., Solomon, S., Pahlavan, H. A., & Lin, P. 2019,
 524 Environmental Research Letters, 14, 114026,
 525 doi: [10.1088/1748-9326/ab4de7](https://doi.org/10.1088/1748-9326/ab4de7)
 526 Gaia Collaboration, Brown, A. G. A., Vallenari, A., et al.
 527 2016, A&A, 595, A2, doi: [10.1051/0004-6361/201629512](https://doi.org/10.1051/0004-6361/201629512)
 528 Garcia, R. R., & Randel, W. J. 2008, Journal of
 529 Atmospheric Sciences, 65, 2731,
 530 doi: [10.1175/2008JAS2712.1](https://doi.org/10.1175/2008JAS2712.1)
 531 Gettelman, A., Mills, M. J., Kinnison, D. E., et al. 2019,
 532 Journal of Geophysical Research (Atmospheres), 124,
 533 12,380, doi: [10.1029/2019JD030943](https://doi.org/10.1029/2019JD030943)
 534 Greene, T. P., Bell, T. J., Ducrot, E., et al. 2023, Nature,
 535 618, 39, doi: [10.1038/s41586-023-05951-7](https://doi.org/10.1038/s41586-023-05951-7)
 536 Grenfell, J. L., Stracke, B., Patzer, B., Titz, R., & Rauer,
 537 H. 2006, International Journal of Astrobiology, 5, 295,
 538 doi: [10.1017/S1473550406003478](https://doi.org/10.1017/S1473550406003478)
 539 Grenfell, J. L., Grießmeier, J.-M., von Paris, P., et al. 2012,
 540 Astrobiology, 12, 1109, doi: [10.1089/ast.2011.0682](https://doi.org/10.1089/ast.2011.0682)
 541 Grenfell, J. L., Gebauer, S., Godolt, M., et al. 2013,
 542 Astrobiology, 13, 415, doi: [10.1089/ast.2012.0926](https://doi.org/10.1089/ast.2012.0926)
 543 Grimm, S. L., Demory, B.-O., Gillon, M., et al. 2018, A&A,
 544 613, A68, doi: [10.1051/0004-6361/201732233](https://doi.org/10.1051/0004-6361/201732233)
 545 Guzel-Seydim, Z. B., Greene, A. K., & Seydim, A. 2004,
 546 LWT-Food Science and Technology, 37, 453
 547 Haagen-Smit, A. J. 1952, Industrial & Engineering
 548 Chemistry, 44, 1342
 549 Harman, C. E., Felton, R., Hu, R., et al. 2018, ApJ, 866,
 550 56, doi: [10.3847/1538-4357/aadd9b](https://doi.org/10.3847/1538-4357/aadd9b)
 551 Harman, C. E., Schwieterman, E. W., Schottelkotte, J. C.,
 552 & Kasting, J. F. 2015, ApJ, 812, 137,
 553 doi: [10.1088/0004-637X/812/2/137](https://doi.org/10.1088/0004-637X/812/2/137)
 554 Helming, D., Ganzeveld, L., Butler, T., & Oltmans, S. J.
 555 2007, Atmospheric Chemistry & Physics, 7, 15,
 556 doi: [10.5194/acp-7-15-2007](https://doi.org/10.5194/acp-7-15-2007)
 557 Iriti, M., & Faoro, F. 2007, Water Air and Soil Pollution,
 558 187, 285, doi: [10.1007/s11270-007-9517-7](https://doi.org/10.1007/s11270-007-9517-7)
 559 Ji, A., Kasting, J., Cooke, G., Marsh, D., & Tsagaridis, K.
 560 2023, Royal Society Open Science, 10, 230056
 561 Ji, A., Kasting, J. F., Cooke, G. J., Marsh, D. R., &
 562 Tsagaridis, K. 2023, Royal Society Open Science, 10,
 563 230056, doi: [10.1098/rsos.230056](https://doi.org/10.1098/rsos.230056)
 564 Joshi, M. M., Haberle, R. M., & Reynolds, R. T. 1997,
 565 Icarus, 129, 450, doi: [10.1006/icar.1997.5793](https://doi.org/10.1006/icar.1997.5793)
 566 Kaltenegger, L., & Sasselov, D. 2010, ApJ, 708, 1162,
 567 doi: [10.1088/0004-637X/708/2/1162](https://doi.org/10.1088/0004-637X/708/2/1162)
 568 Kasting, J. F., Whitmire, D. P., & Reynolds, R. T. 1993,
 569 Icarus, 101, 108, doi: [10.1006/icar.1993.1010](https://doi.org/10.1006/icar.1993.1010)
 570 Kim, J.-G., Yousef, A. E., & Dave, S. 1999, Journal of food
 571 protection, 62, 1071
 572 Kishimoto, N., & Arai, H. 2022, Ozone: Science &
 573 Engineering, 44, 265
 574 Klaunig, J. E., Kamendulis, L. M., & Hocevar, B. A. 2010,
 575 Toxicologic pathology, 38, 96
 576 Kleinböhl, A., Willacy, K., Friedson, A. J., Chen, P., &
 577 Swain, M. R. 2018, ApJ, 862, 92,
 578 doi: [10.3847/1538-4357/aaca36](https://doi.org/10.3847/1538-4357/aaca36)
 579 Kopparapu, R., Arney, G., Haqq-Misra, J., Lustig-Yaeger,
 580 J., & Villanueva, G. 2021, ApJ, 908, 164,
 581 doi: [10.3847/1538-4357/abd7f7](https://doi.org/10.3847/1538-4357/abd7f7)
 582 Kozakis, T., & Kaltenegger, L. 2020, AJ, 160, 225,
 583 doi: [10.3847/1538-3881/abb9ac](https://doi.org/10.3847/1538-3881/abb9ac)
 584 Kozakis, T., Kaltenegger, L., & Hoard, D. W. 2018, ApJ,
 585 862, 69, doi: [10.3847/1538-4357/aacbc7](https://doi.org/10.3847/1538-4357/aacbc7)
 586 Kozakis, T., Mendonça, J. M., & Buchhave, L. A. 2022,
 587 A&A, 665, A156, doi: [10.1051/0004-6361/202244164](https://doi.org/10.1051/0004-6361/202244164)
 588 Large, R. R., Mukherjee, I., Gregory, D., et al. 2019,
 589 Mineralium Deposita, 54, 485,
 590 doi: [10.1007/s00126-019-00873-9](https://doi.org/10.1007/s00126-019-00873-9)
 591 Loyd, R. O. P., France, K., Youngblood, A., et al. 2016,
 592 ApJ, 824, 102, doi: [10.3847/0004-637X/824/2/102](https://doi.org/10.3847/0004-637X/824/2/102)
 593 Luger, R., & Barnes, R. 2015, in American Astronomical
 594 Society Meeting Abstracts, Vol. 225, American
 595 Astronomical Society Meeting Abstracts #225, 407.04
 596 Lushchak, V. I. 2011, Aquatic toxicology, 101, 13
 597 Lykkesfeldt, J., & Svendsen, O. 2007, The veterinary
 598 journal, 173, 502
 599 Lyons, T. W., Diamond, C. W., Planavsky, N. J.,
 600 Reinhard, C. T., & Li, C. 2021, Astrobiology, 21, 906,
 601 doi: [10.1089/ast.2020.2418](https://doi.org/10.1089/ast.2020.2418)
 602 Madhusudhan, N., Piette, A. A. A., & Constantinou, S.
 603 2021, ApJ, 918, 1, doi: [10.3847/1538-4357/abfd9c](https://doi.org/10.3847/1538-4357/abfd9c)

- 604 Malashock, D. A., Delang, M. N., Becker, J. S., et al. 2022,
 605 *The Lancet Planetary Health*, 6, e958
- 606 Malashock, D. A., DeLang, M. N., Becker, J. S., et al. 2022,
 607 *Environmental Research Letters*, 17, 054023,
 608 doi: [10.1088/1748-9326/ac66f3](https://doi.org/10.1088/1748-9326/ac66f3)
- 609 McNaught, A. D., Wilkinson, A., et al. 1997, Compendium
 610 of chemical terminology, Vol. 1669 (Blackwell Science
 611 Oxford)
- 612 Méndez, A., Rivera-Valentín, E. G., Schulze-Makuch, D.,
 613 et al. 2021, *Astrobiology*, 21, 1017,
 614 doi: [10.1089/ast.2020.2342](https://doi.org/10.1089/ast.2020.2342)
- 615 Menzel, D. B. 1984
- 616 Najafi, M. B. H., & Khodaparast, M. H. 2009, *Food
 617 control*, 20, 27
- 618 Nuvolone, D., Petri, D., & Voller, F. 2018, *Environmental
 619 Science and Pollution Research*, 25, 8074
- 620 Otegi, J. F., Bouchy, F., & Helled, R. 2020, *A&A*, 634,
 621 A43, doi: [10.1051/0004-6361/201936482](https://doi.org/10.1051/0004-6361/201936482)
- 622 Padro, J. 1996, *Atmospheric Environment*, 30, 2363,
 623 doi: [10.1016/1352-2310\(95\)00352-5](https://doi.org/10.1016/1352-2310(95)00352-5)
- 624 Peacock, S. 2020, Habitable Zones and M dwarf Activity
 625 across Time ("HAZMAT"), Version 1, STScI/MAST,
 626 doi: [10.17909/T9-J6BZ-5G89](https://doi.org/10.17909/T9-J6BZ-5G89)
- 627 Peacock, S., Barman, T., Shkolnik, E. L., Hauschildt, P. H.,
 628 & Baron, E. 2019, *ApJ*, 871, 235,
 629 doi: [10.3847/1538-4357/aaf891](https://doi.org/10.3847/1538-4357/aaf891)
- 630 Pierrehumbert, R. T., & Hammond, M. 2019, *Annual
 631 Review of Fluid Mechanics*, 51, 275,
 632 doi: [10.1146/annurev-fluid-010518-040516](https://doi.org/10.1146/annurev-fluid-010518-040516)
- 633 Pineda, J. S., Youngblood, A., & France, K. 2021, *ApJ*,
 634 918, 40, doi: [10.3847/1538-4357/ac0aea](https://doi.org/10.3847/1538-4357/ac0aea)
- 635 Premjit, Y., Sruthi, N., Pandiselvam, R., & Kothakota, A.
 636 2022, *Comprehensive Reviews in Food Science and Food
 637 Safety*, 21, 1054
- 638 Proedrou, E., & Hocke, K. 2016, *Earth, Planets and Space*,
 639 68, 96, doi: [10.1186/s40623-016-0461-x](https://doi.org/10.1186/s40623-016-0461-x)
- 640 Ramirez, R. M. 2020, *Scientific Reports*, 10, 7432,
 641 doi: [10.1038/s41598-020-64436-z](https://doi.org/10.1038/s41598-020-64436-z)
- 642 Reinhard, C. T., Olson, S. L., Schwieterman, E. W., &
 643 Lyons, T. W. 2017, *Astrobiology*, 17, 287,
 644 doi: [10.1089/ast.2016.1598](https://doi.org/10.1089/ast.2016.1598)
- 645 Renaud, J. P., Henning, W. G., Saxena, P., et al. 2021,
 646 *PSJ*, 2, 4, doi: [10.3847/PSJ/abc0f3](https://doi.org/10.3847/PSJ/abc0f3)
- 647 Ribas, I., Bolmont, E., Selsis, F., et al. 2016, *A&A*, 596,
 648 A111, doi: [10.1051/0004-6361/201629576](https://doi.org/10.1051/0004-6361/201629576)
- 649 Ridgway, R. J., Zamyatina, M., Mayne, N. J., et al. 2023,
 650 *MNRAS*, 518, 2472, doi: [10.1093/mnras/stac3105](https://doi.org/10.1093/mnras/stac3105)
- 651 Rojas-Valencia, M. 2011, *Virus*, 3, 263
- 652 Safonova, M., Mathur, A., Basak, S., Bora, K., & Agrawal,
 653 S. 2021, *European Physical Journal Special Topics*, 230,
 654 2207, doi: [10.1140/epjs/s11734-021-00211-z](https://doi.org/10.1140/epjs/s11734-021-00211-z)
- 655 Sandu, A., Verwer, J., Blom, J., et al. 1997, *Atmospheric
 656 environment*, 31, 3459
- 657 Schwieterman, E. W., Reinhard, C. T., Olson, S. L.,
 658 Harman, C. E., & Lyons, T. W. 2019, *ApJ*, 878, 19,
 659 doi: [10.3847/1538-4357/ab1d52](https://doi.org/10.3847/1538-4357/ab1d52)
- 660 Schwieterman, E. W., Meadows, V. S., Domagal-Goldman,
 661 S. D., et al. 2016, *ApJL*, 819, L13,
 662 doi: [10.3847/2041-8205/819/1/L13](https://doi.org/10.3847/2041-8205/819/1/L13)
- 663 Segura, A., Meadows, V. S., Kasting, J. F., Crisp, D., &
 664 Cohen, M. 2007, *A&A*, 472, 665,
 665 doi: [10.1051/0004-6361:20066663](https://doi.org/10.1051/0004-6361:20066663)
- 666 Segura, A., Walkowicz, L. M., Meadows, V., Kasting, J., &
 667 Hawley, S. 2010, *Astrobiology*, 10, 751,
 668 doi: [10.1089/ast.2009.0376](https://doi.org/10.1089/ast.2009.0376)
- 669 Sergeev, D. E., Mayne, N. J., Bendall, T., et al. 2023,
 670 *Geoscientific Model Development*, 16, 5601,
 671 doi: [10.5194/gmd-16-5601-2023](https://doi.org/10.5194/gmd-16-5601-2023)
- 672 Sharkey, T. D., Wiberley, A. E., & Donohue, A. R. 2008,
 673 *Annals of botany*, 101, 5
- 674 Showman, A. P., & Polvani, L. M. 2011, *ApJ*, 738, 71,
 675 doi: [10.1088/0004-637X/738/1/71](https://doi.org/10.1088/0004-637X/738/1/71)
- 676 Sies, H., Berndt, C., & Jones, D. P. 2017, *Annual review of
 677 biochemistry*, 86, 715
- 678 Sillman, S. 1999, *Atmospheric Environment*, 33, 1821
- 679 Silva, R. A., West, J. J., Zhang, Y., et al. 2013,
 680 *Environmental Research Letters*, 8, 034005
- 681 Squire, O. J., Archibald, A. T., Abraham, N. L., et al.
 682 2014, *Atmospheric Chemistry & Physics*, 14, 1011,
 683 doi: [10.5194/acp-14-1011-2014](https://doi.org/10.5194/acp-14-1011-2014)
- 684 Steadman, J. A., Large, R. R., Blamey, N. J., et al. 2020,
 685 *Precambrian Research*, 343, 105722,
 686 doi: [10.1016/j.precamres.2020.105722](https://doi.org/10.1016/j.precamres.2020.105722)
- 687 Stokinger, H. 1965, *Archives of Environmental Health: An
 688 International Journal*, 10, 719
- 689 Sun, H. Z., Yu, P., Lan, C., et al. 2022, *The Innovation*, 3,
 690 100246, doi: [10.1016/j.xinn.2022.100246](https://doi.org/10.1016/j.xinn.2022.100246)
- 691 Tabataba-Vakili, F., Grenfell, J. L., Grießmeier, J. M., &
 692 Rauer, H. 2016, *A&A*, 585, A96,
 693 doi: [10.1051/0004-6361/201425602](https://doi.org/10.1051/0004-6361/201425602)
- 694 Tilley, M. A., Segura, A., Meadows, V., Hawley, S., &
 695 Davenport, J. 2019, *Astrobiology*, 19, 64,
 696 doi: [10.1089/ast.2017.1794](https://doi.org/10.1089/ast.2017.1794)
- 697 Tjoa, J. N. K. Y., Mueller, M., & van der Tak, F. F. S.
 698 2020, *A&A*, 636, A50, doi: [10.1051/0004-6361/201937035](https://doi.org/10.1051/0004-6361/201937035)
- 699 Truitt, A. R., Young, P. A., Walker, S. I., & Spacek, A.
 700 2020, *AJ*, 159, 55, doi: [10.3847/1538-3881/ab4e93](https://doi.org/10.3847/1538-3881/ab4e93)

- 701 Turbet, M., Fauchez, T. J., Sergeev, D. E., et al. 2022, PSJ, 721 Wilson, D. J., Froning, C., Duvvuri, G., et al. 2021a,
 702 3, 211, doi: [10.3847/PSJ/ac6cf0](https://doi.org/10.3847/PSJ/ac6cf0) 722 Mega-MUSCLES Semi-empirical SED of TRAPPIST-1,
 703 Turner, M. C., Jerrett, M., Pope III, C. A., et al. 2016, 723 Version 1, Zenodo.
 704 American journal of respiratory and critical care
 705 medicine, 193, 1134
 706 Val Martin, M., Heald, C. L., & Arnold, S. R. 2014,
 707 Geophys. Res. Lett., 41, 2988,
 708 doi: [10.1002/2014GL059651](https://doi.org/10.1002/2014GL059651)
 709 Valavanidis, A., Vlachogianni, T., Fiotakis, K., & Loridas,
 710 S. 2013, International journal of environmental research
 711 and public health, 10, 3886
 712 Way, M. J., Aleinov, I., Amundsen, D. S., et al. 2017,
 713 ApJS, 231, 12, doi: [10.3847/1538-4365/aa7a06](https://doi.org/10.3847/1538-4365/aa7a06)
 714 Wert, E. C., Lew, J., & Rakness, K. L. 2017,
 715 Journal-American Water Works Association, 109, E302
 716 Wesely, M. L. 1989, Atmospheric Environment, 23, 1293,
 717 doi: [10.1016/0004-6981\(89\)90153-4](https://doi.org/10.1016/0004-6981(89)90153-4)
 718 Wesely, M. L., & Hicks, B. B. 2000, Atmospheric
 719 Environment, 34, 2261,
 720 doi: [10.1016/S1352-2310\(99\)00467-7](https://doi.org/10.1016/S1352-2310(99)00467-7)
 721 Wilson, D. J., Froning, C., Duvvuri, G., et al. 2021a,
 722 Mega-MUSCLES Semi-empirical SED of TRAPPIST-1,
 723 Version 1, Zenodo.
 724 <https://doi.org/10.5281/zenodo.4556130>
 725 Wilson, D. J., Froning, C. S., Duvvuri, G. M., et al. 2021b,
 726 ApJ, 911, 18, doi: [10.3847/1538-4357/abe771](https://doi.org/10.3847/1538-4357/abe771)
 727 Wordsworth, R., & Pierrehumbert, R. 2014, ApJL, 785,
 728 L20, doi: [10.1088/2041-8205/785/2/L20](https://doi.org/10.1088/2041-8205/785/2/L20)
 729 World Health Organization, et al. 2000, Air quality
 730 guidelines for Europe (World Health Organization.
 731 Regional Office for Europe)
 732 Yassin Jaziri, A., Charnay, B., Selsis, F., Leconte, J., &
 733 Lefèvre, F. 2022, Climate of the Past, 18, 2421,
 734 doi: [10.5194/cp-18-2421-2022](https://doi.org/10.5194/cp-18-2421-2022)
 735 Yates, J. S., Palmer, P. I., Manners, J., et al. 2020,
 736 MNRAS, 492, 1691, doi: [10.1093/mnras/stz3520](https://doi.org/10.1093/mnras/stz3520)
 737 Youngblood, A., France, K., Loyd, R. O. P., et al. 2016,
 738 ApJ, 824, 101, doi: [10.3847/0004-637X/824/2/101](https://doi.org/10.3847/0004-637X/824/2/101)
 739 Zieba, S., Kreidberg, L., Ducrot, E., et al. 2023, arXiv
 740 e-prints, arXiv:2306.10150,
 741 doi: [10.48550/arXiv.2306.10150](https://doi.org/10.48550/arXiv.2306.10150)